# DESIGN AND SIMULATION OF A HYBRID UAV

PROJECT REPORT

Submitted by

**GEMMY GEO THOMAS (KTE17ME025)**

**LAVAKUMAR V (KTE17ME039)**

**M MIDHUN NAIR (KTE17ME042)**

**NIKHIL SCARIA (KTE16ME042)**

To

APJ Abdul Kalam Technological University

In partial fulfilment of the requirements for the award of the Degree

Of

Bachelor of Technology

In

*Mechanical Engineering*


**Department of Mechanical Engineering**

RAJIV GANDHI INSTITUTE OF TECHNOLOGY

KOTTAYAM

JUNE, 2021

# DECLARATION

We, the undersigned, hereby declare that the project report "Design and Simulation of a Hybrid UAV", submitted for partial fulfillment of the requirements for the award of Degree of Bachelor of Technology of the APJ Abdul Kalam Technological University, Kerala, is a bonafide work done by us, under supervision of Assistant Professor Antony J K. This submission represents our ideas in our own words, and where ideas or words of others have been included, we have adequately and accurately cited and referenced the original sources.

We also declare that we have adhered to the ethics of academic honesty and integrity and have not misrepresented or fabricated any data, idea, fact or source in our submission. We understand that any violation of the above will be a cause for disciplinary action by the institute and/or the University and can also evoke penal action from the sources which have thus not been properly cited or from whom proper permission has not been obtained. This report has not been previously formed for awarding any degree, diploma, or similar title of any other University.

Pampady
Date: 14-07-2021

Gemmy Geo Thomas

Lavakumar V

M Midhun Nair

Nikhil Scaria

# DEPARTMENT OF MECHANICAL ENGINEERING

RAJIV GANDHI INSTITUTE OF TECHNOLOGY

GOVERNMENT ENGINEERING COLLEGE, KOTTAYAM
686501

## CERTIFICATE

This is to certify that the Project entitled **"DESIGN AND SIMULATION OF A HYBRID UAV"** is a bona fide record of the Graduate Project presented by **GEMMY GEO THOMAS, LAVAKUMAR V, M MIDHUN NAIR** and **NIKHIL SCARIA** of Eighth Semester during the year 2020-2021. This report is submitted to APJ Abdul Kalam Technological University, Thiruvananthapuram in partial fulfilment of the requirements for the award of the degree of Bachelor of Technology in Mechanical Engineering.

ANTONY J. K.
Assistant Professor
Dept. of Mechanical Engineering
RIT, Kottayam
(Project Guide)

Professor and HOD
Dept. of Mechanical Engineering
RIT, Kottayam

# ACKNOWLEDGEMENT

On presenting the project report, we wish to express our deep and profound feeling of gratitude towards several people who have contributed to the successful completion of our project.

First, we express our deep gratitude to Lord Almighty, the supreme guide, for bestowing his blessing through each phase of our work. We would like to thank **Prof. ANTONY J K** (Department of Mechanical Engineering, RIT Kottayam) for his consistent guidance and inspiration throughout our project work. We also express our heartfelt gratitude to **Dr. A. RAMESH** (Head of the Department and Professor of Mechanical Engineering, RIT Kottayam) and **Dr. JALAJA M.J** (Principal, RIT Kottayam) for rendering all possible help and support during our project. Last, but not the least, we are grateful to the management, all the staff members of RIT Kottayam for their cooperation and help extended during our project. We would also like to thank all our alumni, friends, family members for their encouragement, inspiration, and moral support without which this work would have never been possible.

Gemmy Geo Thomas

Lavakumar V

M Midhun Nair

Nikhil Scaria

# ABSTRACT

Urban air mobility is a broad umbrella term used to group various aviation-based mobility solutions and ideas in urban scenarios. It is a field that is quickly gaining attention, especially from big players such as Airbus, Boeing, and Amazon, due to the various attractive advantages it offers such as traffic decongestion, quick transport of people and goods, etc. Multiple forays are being conducted for implementing these mobility ideas for various applications. There is simultaneous research into the development of manned and unmanned solutions for various applications. For this project, we plan to design and analyse a hybrid UAV for the purpose of transporting medium-weight medical cargo. For conforming to the practical limitations set forth by its proposed application, the UAV is intended to possess VTOL capabilities but also have a fixed-wing design to extend its range. Therefore, the UAV is intended to be a hybrid of a multirotor and fixed-wing aircraft. The challenge faced in this project was the optimization of the design of this prototype to fulfil the intended design objectives.

*Keywords: Hybrid UAV, VTOL UAV, quadplane, aviation, transportation*

# CONTENTS

# LIST OF FIGURES

# LIST OF TABLES

# CHAPTER 1

# INTRODUCTION

During the last two to three decades, Unmanned Aerial Vehicles (UAVs) have experienced tremendous development. Miniature UAV platforms are dominated by two main types, i.e., fixed-wing conventional aircrafts and Vertical Take-Off and Landing (VTOL) aircrafts, and each type have its own inherent limitations such as flexibility, payload, endurance, etc. A new and promising trend is to develop fixed-wing VTOL UAVs or the so-called Hybrid UAVs, which can inherit the advantages of both and thus have the ability of vertical take-off and landing as well as high cruising speed and enhanced endurance. The advantages of combining fixed-wing and VTOL capabilities in a single aircraft have led this field to be a lucrative frontier for many aerospace and aviation industries. Over the years, there have been several attempts to build manned hybrid aircraft such as Bell Boeing V-22 Osprey, Vertol VZ-2, Sikorsky X-wing, Convair XFY Pogo, and Harrier GR7, as shown in Fig. 1(a) to 1(e) respectively [1][2][3].

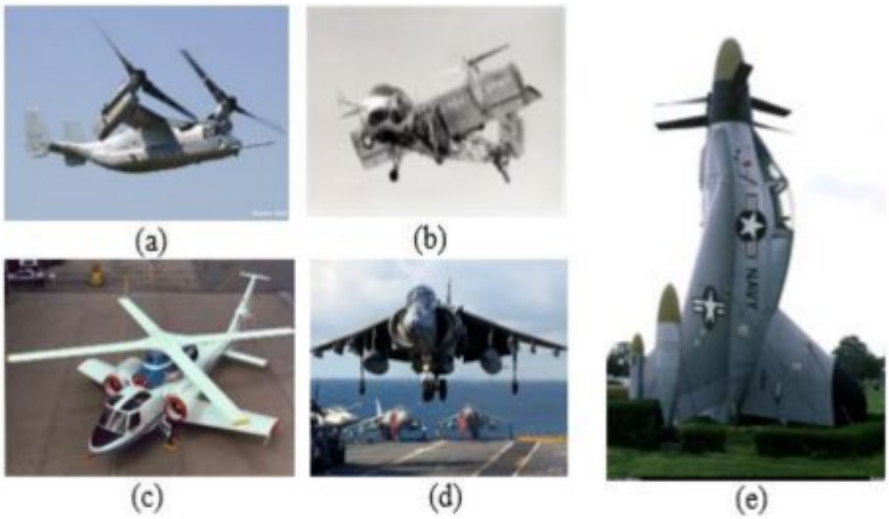


Fig. 1.1. Hybrid Aircrafts

Some of the attempts did succeed, and these aircrafts are still operating up to the moment, such as V22-Osprey and Harrier GR7. Nevertheless, within the last four years, the concept invaded the UAV field as several research groups documented their pioneer work in literature, and a couple of companies even commercialized the idea. It is believed that the hybrid UAVs will be having a bright future and will promptly dominate the miniature UAV market. Still, in its infancy, there is a huge space for the miniature hybrid UAVs to become more mature in terms of design philosophy, dynamics modelling, control, guidance, navigation, robustness, etc.

## 1.1. OBJECTIVE

The main purpose was to design and construct a hybrid UAV which had both VTOL and long-range capabilities. Our focus was mainly on the medical transportation sector. In a vast country like India, even today many people are drastically affected by the availability of medicines and other medical equipment, and most of the modern norms of medical science are still unknown to a large part of Indian population. With the implementation of hybrid UAVs, such a system would revolutionize the medical field by incorporating affordable and accessible transportation, thereby decreasing the death rates that happen through insufficient transportation for medical emergencies.

But due to COVID-19, we were not able to proceed with the construction part and focused more on analyses and simulation. The main challenges were the designing of the control systems and simulation of the hybrid UAV.

## 1.2. HYBRID UAV

Mainly UAVs are of two types: fixed-wing UAV and rotary-wing UAV. Both types of UAVs have their advantages and disadvantages according to the requirement. The fixed-wing UAV has high efficiency, long-endurance, and range but requires a runway for take-off and landing, thus limiting its operation. On the other hand, rotary-wing UAVs can take off and land vertically, so in this way, it has an advantage over fixed-wing UAVs, but it does not have long endurance and range. It is still a challenge to design a UAV having both high endurance and range, and at the same time with vertical take-off and landing capabilities. To some extent, the hybrid VTOLs are the capable solution that is conceptualized based on both fixed and rotary-wing UAVs as a single unit [4]. People are using several types of VTOL UAVs such as tail sitter, tiltrotor, and hybrid VTOL UAVs. A tail-sitter VTOL UAV takes off vertically on its tail, and the whole aircraft tilts horizontally. Many researchers have studied its design and modelling. Tail-sitter uses the same motors for both hovering and level flight. In the tilt-rotor VTOL UAV, the generation of lift and forward thrust is done using the same propulsion system, and unlike in the tail-sitter rotor, it only tilts its rotors.

Fig. 1.2. A Hybrid VTOL UAV

For the hybrid VTOL UAV (Fig. 1.2.), two independent propulsion systems are used for hovering and level flight. Four lifting rotors generate the lift force during the take-off while the push motor is turned off, and the aircraft behaves as a quadrotor.

## 1.3. SIGNIFICANCE

Aerial vehicles have proved their usefulness in the military (combat, deployment of units, patrolling, surveillance, reconnaissance, etc.) and civil areas (transport, search and rescue, firefighting, etc.) on various applications over a hundred years while enhancing their capabilities over time and fulfilling ever-changing mission requirements. UAVs offer a unique set of advantages compared to piloted aircraft with smaller, safer, and lighter platforms. Future UAVs are expected to perform much more extended missions with higher manoeuvrability and higher degrees of autonomy [5]. Various capabilities like VTOL, hover, level flight, and transitions between hover and level flight can be expected from a UAV platform, according to mission requirements. When VTOL and hovering are required, then rotary-wing aircraft such as helicopters, multirotor and ducted fans are most optimal. However, if endurance is of priority, then a fixed-wing type will most likely be preferred due to the efficiency of level flight. When both features are desired, then a VTOL-UAV with level flight capability becomes the best option. VTOL capability removes the need for runway or launch/recovery equipment and provides flexibility to operate in any theatre, whereas level flight capability allows efficient range and endurance flight. An aerial vehicle designed to possess the strengths of both a rotary and fixed-wing aircraft will have both advantages in one platform. Transition manoeuvres between hover and level flight is of primary concern for VTOL aircraft that are capable of level

flight. In this study, the design and implementation of the control system of a VTOL aircraft with level flight capability is considered.

## 1.4. ENVIRONMENT AND SUSTAINABILITY

The topic of environment and sustainability is mostly characterized by the lack of solid scientific evidence and uncertainties about the environmental impact of drones. While environmental issues made up less than 1% of all expected benefits from 2013 to 2015, they made up 16.5% in 2018[6]. Similarly, there are almost no proposed solutions concerning drones' environmental impact from 2013 to 2016, but they make up over 5% of all proposed solutions in 2017 and 2018[7]. The number of quotations about potential environmental problems is slightly more constant, but there is still a notable increase from 7.1% of all citations addressed in 2015 to 10.8% in 2018[8]. Most quotations concerning expected environmental benefits describe drones as a more environment friendly technology for both logistics and passenger transportation. The main reason is the fact that drones have a fully electric transportation technology. This is either expressed in rather general terms or in comparison to other (conventional) transportation technologies. 'Air taxis' are, for instance, considered to reduce carbon/noise footprint in comparison to fossil-fuelled helicopters. In a one-trip-per-item scenario where a drone transports a relatively light load, delivery drones have a significantly higher energy efficiency than, for example, diesel vans. However, as soon as several parcels must be delivered, conventional delivery methods remain more energy-efficient, especially in cases where recipients can be grouped along routes or when service zones are distant. Most scientists, therefore, propose that "a blended system would perform best (emit the least) with drones serving nearby addresses and trucks delivering to ones farther." The two most frequently discussed potential environmental problems are dangers to wildlife and the uncertainties regarding actual energy efficiencies and emissions of delivery drones. While some people see drones as an opportunity for sustainable mobility, for others, they represent various uncertainties. As a result, people caution that the impact of drone delivery systems on the environment is still in question, and environmental sustainability should be assessed under widespread aerial transportation and through life cycle assessment. It is therefore criticized that only a few scholarly analyses have been conducted to determine the actual $CO_2$ reduction when drones are used in cities. Most proposed environmental solutions look at very specific sustainability issues related to the use of drone technology and provide suggestions for improvements. These include the strategic construction of drone warehouses or the use of green energy to charge the drone. Interestingly, most solutions do not address the major issues

identified in the context of environmental problems. In fact, only two suggestions deal with the protection of wildlife, and none deal explicitly with the issue of providing more certainty about the positive environmental impact of drone technology.

# CHAPTER 2

# DESIGN METHODOLOGY

## 2.1. MISSION REQUIREMENTS

The UAV design process was initiated by identifying the desired design requirements including the mission profile and required mission specifications. The envisioned goal is for the UAV to achieve high speed, enhance its operational range, while maintaining its current VTOL capabilities including its unique pitch hover and maneuver abilities in confined spaces.

### 2.1.1. MISSION PROFILE

A typical mission profile of the UAV can be described in a sequence of six steps as illustrated in Fig. 2.1.

1. Take-off (vertical)
2. Hovering.
3. Transition from helicopter flight mode to fixed-wing flight mode.
4. Cruise as a fixed-wing UAV.
5. Transition from fixed-wing flight mode to helicopter flight mode.
6. Landing (vertical)

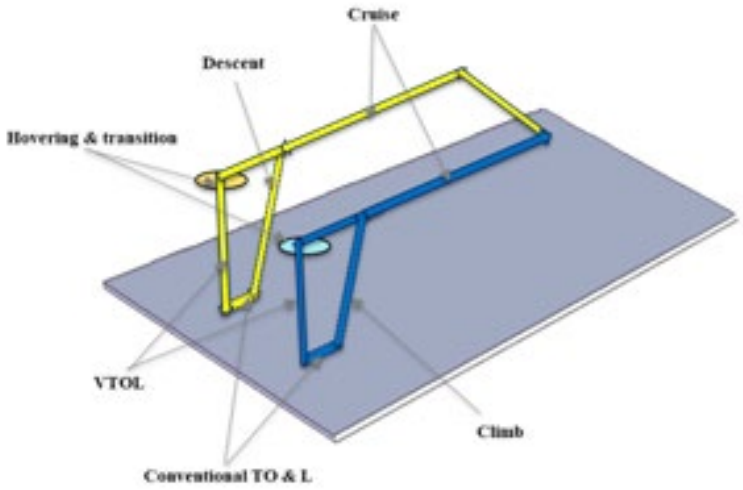


Fig. 2.1. Mission profile

### 2.1.2. MISSION SPECIFICATIONS

The required performance mission specifications in quadrotor and fixed-wing modes have been selected as presented in Table 2.1. These performance mission specifications were selected as they illustrate typical desired specifications that will provide a good test bench to develop and analyze the proposed TA design methodology. With the selected mission specifications, one can move towards the first phase of the UAV design process - conceptual design.

Table 2.1. Mission specifications

| Parameter | Value |
|---|---|
| Total Cruise Range | 2.5 km |
| Cruise Altitude | 45 m |
| Payload weight | 1 kg |
| Total Aircraft weight | 6 kg |
| Cruise Velocity | 15 m/s |

## 2.2. ANALYZING SIMILAR SYSTEMS AND CONCEPTUAL DESIGN

Fixed-wing VTOL UAV has the advantages of having less demand for landing space, high agility and high cruising speed compared with traditional air vehicles. It is one of the hotspots of aircraft development. In this phase, we analyzed the technical characteristics of different types of fixed-wing VTOL UAVs, prospected their development trends, and put forward a feasible design plan of the hybrid quadrotor UAV.

In selecting the aircraft's configuration and to reduce the diverse complexities associated with transitional systems, three proposed configurations have been introduced and compared against each other. This step has been based on the available literature results, to identify the most suitable configuration. From these available configurations, the one that was suitable for us was identified. The design is a hybrid between that of a fixed-wing aircraft and a multirotor which makes it VTOL compatible and gives it decent payload carrying and deployment capabilities. The design employs a flying wing for forward flight, with a four-rotor set up for vertical takeoff and landing. Having a multirotor enables it to take off and land in places where a lot of space for take-off and landing might not be available. This essentially means that this aircraft is capable of accessing places that other aircraft might not be able to access. The aircraft is designed to have a wing span of 1.67 m. This makes it suitable to have a very small form

factor when compared to other UAVs. The rotors are arranged in an H frame with central beam linking a front motor boom to a rear motor boom on both sides.

## 2.3. PRELIMINARY SIZING/RESIZING PROCESS

The objectives of the sizing process are to determine the major parameters of mass, geometry, and propulsion of a future aircraft based on a set of design requirements and to refine them using the information about the exact components of the propulsion system and battery. The overall process started from creating the set of performance and mission requirements. The initial geometry, mass, and required parameters of the propulsion system were calculated at this stage. The UAV maximum take-off weight was estimated based on the weight build up method. In order to calculate, a quick survey to similar fixed-wing UAVs (with a similar payload weight) was conducted. The actual models of electric motors, propellers, and batteries were selected after the basic parameters of propulsion are calculated. The total mass of the aircraft was then updated based on new mass data of motors, propellers, and batteries. The capacity of the battery required to accomplish the mission profile was determined based on the updated mass of the aircraft, power of the motors, propeller diameter, and specific capacity of the battery. Wing and tail geometry of the aircraft were then recalculated using the new total mass value. Previously selected components were compared to new required values at the parameter checking stage. If the difference between selected component's parameter and newly calculated requirement is large, then an alternate component should be selected from the products available in the market. The process is repeated if the difference between mass and power estimated at the initial sizing stage and the resized values is large.

## 2.4. DESIGN, ANALYSIS AND SIMULATION

The next part was the actual designing of the UAV. This work was done on the basis of the information collected from previous works. Our primary objective was to determine an airfoil with maximum lift generation under required operating conditions. From the selected airfoil profile, the wing model was generated using SOLIDWORKS. Stability calculations were done and neutral point and lever arm were found. The conceptual design was then developed into the actual CAD model using SOLIDWORKS by considering the critical design parameters. A structural analysis of the wing structure was also performed to check whether the material assigned for wing would be able to withstand the pressure force generated by the air. The simulation part was done using MATLAB Simulink software to model and analyze the UAV

system architecture. Here, we designed the flight control algorithm and ran a simulation of the UAV plant model, while including environmental factors as well.

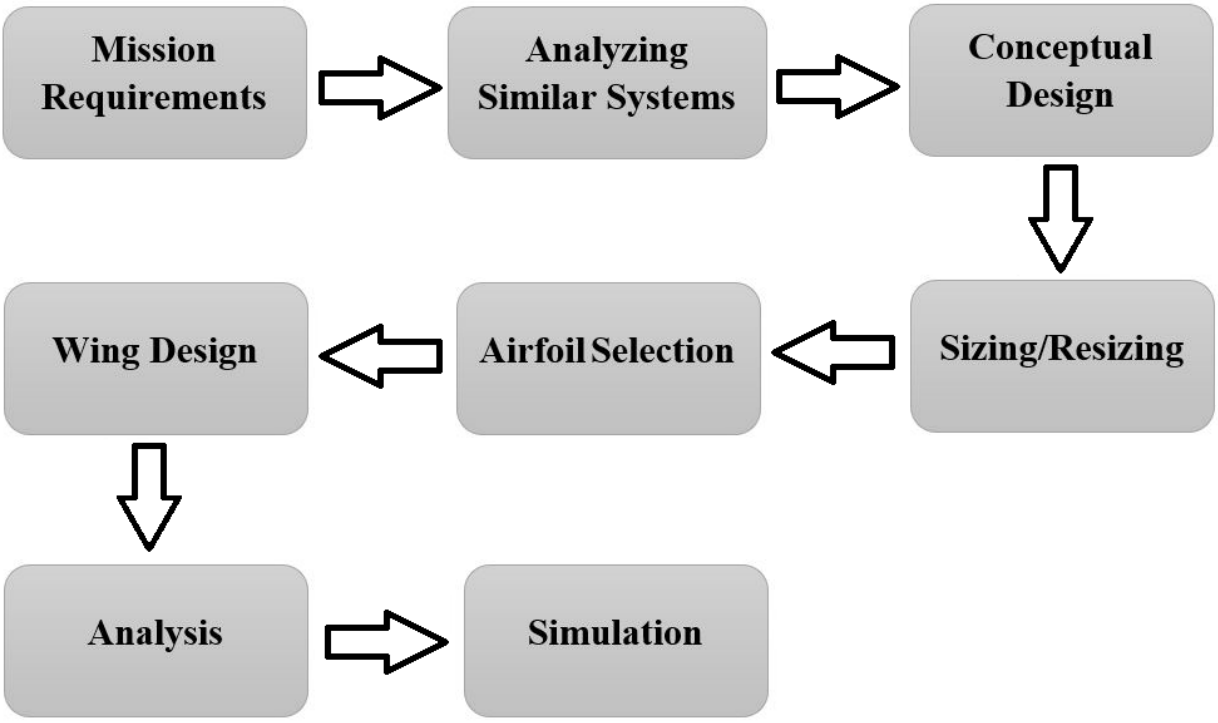


Fig. 2.2. Design Methodology

# CHAPTER 3

# LITERATURE REVIEW

## 3.1. INTRODUCTION TO UAV

An unmanned aerial vehicle (UAV) is an aircraft without any human pilot, crew or passengers on board. UAVs are a component of an unmanned aircraft system (UAS), which additionally includes a ground-based controller and a system of communications with the UAV. The flight of UAVs may operate under remote control by a human operator, as remotely-piloted aircraft (RPA) [9], or with various degrees of autonomy, such as autopilot assistance, up to fully autonomous aircraft that have no provision for human intervention.

UAVs were originally developed through the twentieth century for military missions too "dull, dirty or dangerous" for humans. As control technologies improved and costs fell, they are rapidly finding many more applications in the recent times, including aerial photography, product deliveries, agriculture, policing and surveillance, infrastructure inspections, science, smuggling, and drone racing [9].

They are highly effective in remote operations and have been used in several applications such as law enforcement [10], surveillance [11], search [12], agriculture [13][14], border patrol [15], scientific experiments [16], and mapping [17]. UAVs have been broadly classified as fixed-wing [18] and multirotor aircrafts. Fixed wing UAVs have a simple structure, fly at high speeds and for a longer duration compared to rotary wing UAVs. However, some of the fixed wing UAVs may require a runway for take-off and landing, while those that can be either hand launched or through a catapult mechanism can be landed without a runway. On the other hand, rotary wing UAVs have an advantage of hovering, which is useful for monitoring some regions of interest. Rotary wing UAVs have agile maneuvering capability but at the same time they have high mechanical complexity, low speed and short flight range [19].

Both types of UAVs have their own design limitations. Fixed wing aircraft have good endurance but lack in the capability of taking off and landing vertically while multirotor aircraft have VTOL capabilities but have limited range and a far lesser time of flight than their fixed-wing counterparts. There are studies going at improving the UAV capabilities through innovative designs composed of both Fixed wing and VTOL capabilities [20].

## 3.2. UAVs FOR PARCEL AND PASSENGER TRANSPORTATION

Developments across the recent years have shown that unmanned aerial vehicles (UAV) have the potential to become an iconic technology of the 21st century. They combine three key principles of technological modernity - data processing, autonomy and boundless mobility. They provide access to (new) spaces and enable their analysis with the help of unprecedented methods of data collection. These capabilities, previously a privilege reserved to the military, are now increasingly incorporated into civil domains. Thus, unmanned aerial vehicles generate potential use-cases ranging from surveillance/sensing missions to novel forms of logistics and passenger transportation.

Regardless of their application, UAVs are driven by a general motivation to make processes faster and more flexible, while improving precision and cost-efficiency [21]. As a consequence, the commercial use of drones is associated with vast economic opportunities. Although drones as surveillance/sensor devices are already common in security services, geodesy and agriculture their use as transportation devices is still in its infancy. Nevertheless, from a purely technical perspective delivery drones are already able to lift weights of up to 2–3 kg and conduct flight missions in an urban radius [22]. In addition to that, passenger drones, so called 'air taxis', have already proven their technical ability to transport passengers within or between cities [23]. This does not just illustrate a historical turning point in aviation, but also marks the beginning of a new era, where low level airspace may become the 'third dimension' of transportation.

Against this background, a socio-technical debate exists on the use of civil drones for transportation purposes by evaluating the anticipated barriers, potential problems, proposed solutions and expected benefits that are central to discussions about the technology. The barriers faced by the emerging drone delivery technology are societal implications, safety and security, ethics, environmental issues, public acceptance, urban planning and infrastructure.

The topic of safety and security is characterized by a great problem awareness. This is already quite obvious when considering the key category of potential problems, in which drone-related risks for safety and security form the third largest group of quotations. The topic has gained increasing relevance over the years. Regarding expected benefits related to safety and security issues it is striking that all refer to the use of drones as sensory devices and never to their use as a transportation technology. Obviously, the technology is not anticipated to make transportation more safe and secure. Potential safety and security problems of drone use are

perceived to be a major issue. Air collisions, crashes and malfunctions of software and hardware components could be especially relevant for urban areas. The misuse of drones for criminal or terrorist purposes is also discussed: drones could be used “to smuggle weapons or drugs” or “hacked for consumer data”. The latter aspect was held especially relevant as the inconspicuous nature of drones makes it “difficult for the owner to detect the leak of information and ensure the security of the information as well as claims on ownership”. Proposed solutions offer to either reduce or prevent drones' potential damages. For instance, universal registration of drones in operation might “allow better knowledge on who to prosecute in the event of an incident.” Technical solutions involve geo-fencing and no-fly zones. These block certain areas, buildings or infrastructures from being flown over. The measures are implemented by drone sound detection [24], built-in transponders or software restrictions. Possibilities of drone defense range from interfering signals to launching interception devices and trained birds of prey.

Ethical problems represent the second-largest group of all potential problems in the dataset. The concern of privacy violations is the key issue here. A second, though much smaller group addresses the lack of transparency regarding aims and purposes of drone operations. It is followed by issues of data privacy and the potential of increased surveillance. Proposed solutions for mitigating potential privacy violations include technical and legal strategies. The most frequently discussed technological solution is to make UAVs identifiable through in-built remote identification systems. In addition, some authors suggest integrating preventative measures into drone designs. Such measures include algorithms as well as software designs for real time privacy impact assessments. Other technical approaches comprise geofencing or no fly zones.

The topic of environment and sustainability is mostly characterized by a lack of solid scientific evidence and uncertainties about the environmental impact of drones. The majority of quotations concerning expected environmental benefits describe drones as a more environmentally friendly technology for both logistics and passenger transportation. The main reason is the fact that drones are a fully electric transportation technology. ‘Air taxis’ are for instance considered to reduce carbon/noise footprint in comparison to fossil-fueled helicopters. Assessing the environmental benefits of delivery drones is complex and dependent on the respective deployment scenario. In a one-trip-per-item scenario where a drone transports a relatively light load, delivery drones have a significantly higher energy efficiency than, for example, diesel vans. However, as soon as several parcels have to be delivered conventional

delivery methods remain more energy efficient, especially in cases where recipients can be grouped along routes or when service zones are distant. The two most frequently discussed potential environmental problems are dangers to wildlife and the uncertainties regarding actual energy efficiencies and emissions of delivery drones. The majority of proposed environmental solutions looks at very specific sustainability issues related to the use of drone technology and provides suggestions for improvements. These include the strategic construction of drone warehouses or use of green energy to charge the drones. Interestingly, most solutions do not address the major issues identified in the context of environmental problems.

The analysis provides an interim picture and discursive wrap-up within a highly dynamic field characterized by various uncertainties. As we have shown [25], these uncertainties are compensated (or reflected) by often oversimplified promises and premature evaluations. This calls for an intensification of research efforts and further interdisciplinary inquiry. These inquiries would have the task to promote more comprehensive discussions on expected positive and negative effects of the technology. The results could then support an informed social and legal discourse on which sustainable economic development can be based. Technology assessment and mobility studies do not yet seem to have fully realized the topic's potential relevance.

## 3.3. PLATFORM DESIGN

For now, miniature UAV platforms are dominated by two main types, i.e., fixed-wing conventional aircrafts and Vertical Take-Off and Landing (VTOL) aircrafts, and each type has its own inherent limitations such as flexibility, payload, endurance, and etc. A new and promising trend is to develop fixed-wing VTOL UAV or the so-called Hybrid UAV, which can inherit the advantages of both and thus have the ability of vertical take-off and landing as well as high cruising speed and enhanced endurance. This enables the possibility of performing a wider range of missions or same missions with better performance.

Hybrid UAVs can be generally categorized into two main types: Convertiplanes and Tail-Sitters. Each of them can be further categorized into a few sub-types, depending on the transition mechanism and airframe configuration.

### 3.3.1. CONVERTIPLANE

A convertiplane is a type of hybrid aerial vehicle that takes off, cruises, hovers and lands with the aircrafts reference line remaining horizontal (i.e., the main body configuration does not change during flight). A variety of transition mechanisms are applied to achieve the

conversion from vertical flight to horizontal flight and vice versa. Based on that, convertiplanes can be further categorized into four sub-types: 1) Tilt-Rotors, 2) Tilt-Wings, 3) Rotor-Wings, and 4) Dual Systems.

#### 3.3.1.1. TILT-ROTOR

The primary feature of the Tilt-Rotor aerial vehicle is that the multiple rotors used are mounted on rotating shafts or nacelles. During transition, the rotors tilt gradually towards flight direction providing the aircraft forward speed until level flight mode is achieved. Some Tilt-Rotors might have fixed rotors always directed up, that operate only during vertical flight to provide extra lift for takeoff, landing and hovering. An example of manned Tilt-Rotor is Bell Boeing V-22 Osprey.

Fig. 3.1. Tilt Rotor type UAV

#### 3.3.1.2. TILT-WING

A Tilt-Wing has a similar concept to Tilt-Rotor except that the assembly of the wing tilts instead of the rotors only. During takeoff, landing and hovering, the wings will be directed upwards which makes the aircraft more vulnerable to cross winds. Consequently, the Tilt-Wing requires complicated control mechanisms and higher use of available power to maintain stability during vertical flight. Furthermore, landing on moving deck environments is relatively more difficult compared to Tilt-Rotors. However, since rotors are fixed to wings, this allows various design options for the wing geometry and therefore enhance the aerodynamic performance of the aircraft.

Fig. 3.2. Tilt wing type UAV

### 3.3.1.3. ROTOR-WING

A Rotor-Wing (or Stop-Rotor) is another type of Convertiplane aircrafts where rotary wings spin to provide lift during vertical flight and stop to act like a fixed wing during horizontal flight. The way the Rotor-Wings work makes the possible design configurations minimal which is why most of the Rotor-Wing works show similar design configuration which is close to a helicopter. However, a different design configuration in which the whole-body tilts during transition was detailed in [26] and [27] but no full envelope powered flight test was conducted. Therefore, the implementation of such design might be suspicious due to the lack of historical successes.

Fig. 3.3. Rotor wing type UAV

### 3.3.1.4. DUAL-SYSTEMS

Another type of Convertiplanes which could be referred to as Dual-System implements multiple rotors always directed upwards for vertical flight and another separate tractor or pusher for level flight. Many possible design configurations are possible for this specific type of UAV but due to the huge weight of the aircraft, quad rotors are the most common. The concept of Dual-Systems is very simple to apply in terms of design, controllability, stability

and modeling because the two flight modes could be analyzed separately. However, during horizontal flight, the multiple lifting rotors used for vertical flight are not in operation and add extra weight to the aircraft which results in requiring more power from the tractor or pusher.

Fig. 3.4. Dual system type UAV

### 3.3.2. TAIL-SITTER

A Tail-sitter is an aircraft that takes off and lands vertically on its tail and the whole aircraft tilts forward using differential thrust or control surfaces to achieve horizontal flight. This concept could also be denoted as Tilt-Plane since the whole plane tilts to achieve level flight. Due to its ability to make the transition without the need of extra actuators, this concept is mechanically simple and saves a huge amount of weight when compared to Convertiplanes. Moreover, since tail-sitters land on their tails, they require relatively stronger tails to be able to withstand landing impacts.

Fig. 3.5. Tail sitter type UAV

## 3.4. VTOL TO FW TRANSITION

It is important to point out that there have been a few successful attempts to convert some FW UAVs to take-off and land vertically. But the number is still small and most are done on small scale battery-powered FW UAVs as proof of concept. For military operations, a few successful attempts were made by Jengdu JOUAV Automation Tech. Co. Ltd and by Bluebird Aero Systems in their ThunderB Tactical UAS. Textron Systems Unmanned Systems Service also produced Textron/Aerosonde Hybrid Quadrotor UAV. If more such UAVs can incorporate these dual capabilities, the existing operational envelop of FW UAVs as we know it, can be expanded. To understand the transition phases of flight, it is quite important to look back at the fundamentals of fixed wing flight to make the hybrid UAV capitalize this new flying capability [28]. Fixed-wing aircraft in general, needs some forward airspeed, $V_\infty$, to fly. The area of high pressure created under the wing causes the aircraft to be lifted upwards.

**Strategy 1: Hover to Forward Flight**

The first strategy is to manipulate the speed of the rotors subsequently moving the aircraft forward just like how a typical QD would, until the aircraft travels past the stall speed $V_s$, while maintaining altitude. Notice that, as a matter of choice, this is achieved without using any thrust from the UAV main engine. In this case, the multi-rotors serve two purposes: to hover at a fixed point in space and to provide initial forward speed past $V_s$. Only after the airspeed exceeds $V_s$, the main engine will be throttled up. For this strategy to be successful, the actions from the 4 rotors must produce enough forward speed until the aircraft past $V_s$.

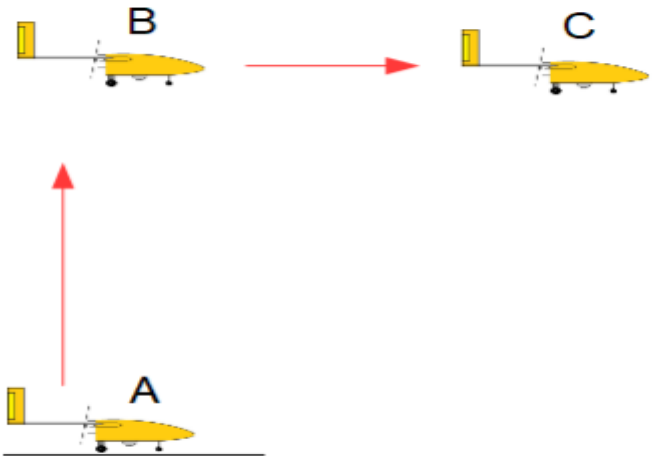


Fig. 3.6. Strategy 1

**Strategy 2: Hover to Forward Flight**

The second strategy is to use the 4 rotors to keep the aircraft steady during hovering in both altitude and attitude. And then apply forward thrust using the main UAV engine causing the forward airspeed, $V_\infty$, to rapidly increase. Once the airspeed past the stall speed, $V_s$, the 4 rotors can stop providing lift for the aircraft. In this scenario, the rotors' role is to maintain altitude and attitude until $V_\infty > V_s$.

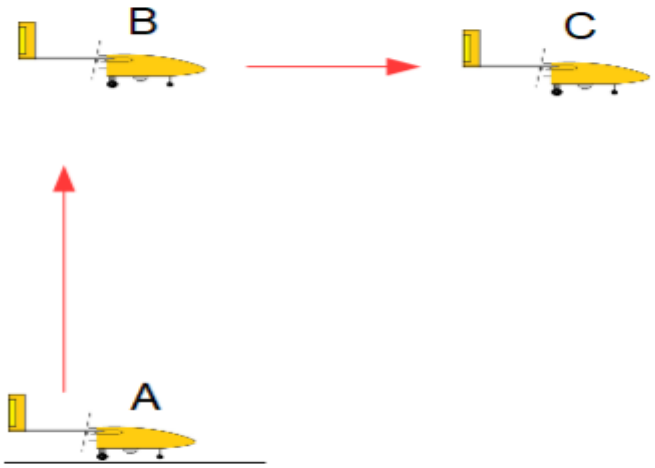


Fig. 3.7. Strategy 2

**Strategy 3: Hover to Forward Flight**

In this method, from hovering position, the 4 spinning rotors will be disengaged to allow the nose of the aircraft to drop and the aircraft is accelerated to past the stall speed ($V_s$) using gravity. If necessary, while gliding, the main engine will be set to full throttle to expedite the build-up of airspeed until past stall speed and forward flight will continue as usual from that point.

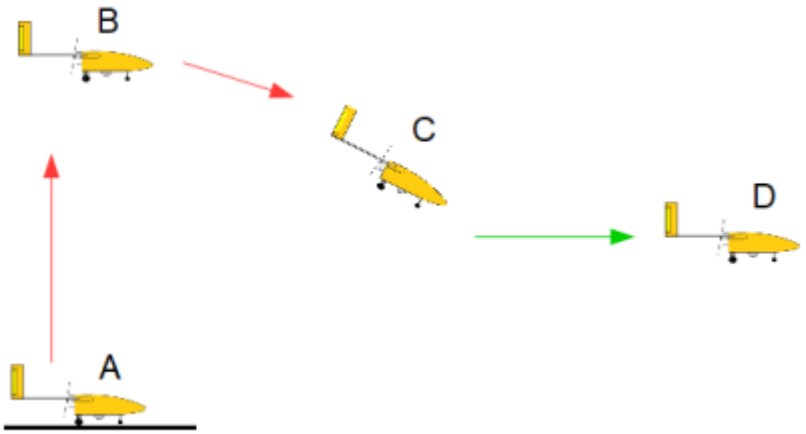


Fig. 3.8. Strategy 3

## 3.5. HYBRID UAV FLIGHT CONTROL TECHNIQUES

The core of the control system depends on the derived dynamics model. The equations of motion are highly complicated and nonlinear. Particularly speaking, the dynamics of the hybrid UAVs can be inherently unstable because it inherits the operation of a fixed-wing and VTOL UAVs. Even if horizontal and vertical modes were analyzed separately, the transition phase remains a critical part of the control system due to the multiple nonlinearities in the model. This is why feedback control is essential, as it ensures more accurate and quicker response to meet the desired reference command.

Flight control system theory deals with the synthesis and analysis of the logic behind which the flight control system is designed. There are two strategies for that, namely the classical control theory and the modern control theory. The former, also known as successive loop closure, considers the decomposition of the states derived from the model to form successive control loops such that the output of the innermost loop (low-level) is linked to the actuators of the UAV. It is important to note that the low-level controllers (innermost) should have a quicker response than the higher ones. For a particular case of hybrid UAVs, the decomposition of the states could result in a low-level attitude controller directly linked to the control surfaces of the UAV. It gets the reference commands from a mid-level velocity controller which gets the reference commands from the high-level position controller. This control theory was implemented in Ducted-Fan Tail-sitters, Tilt-Rotors and Tilt-Wings and other tail-sitters, mainly for hovering.

The second approach, known as modern control, is to design a control system that handles the full dynamics of the UAV. The stability and control specifications can be expressed in terms of a system of first-order differential equations which results in matrix equations that can be solved using commercially available computer software to compute the control gains simultaneously [29] [30]. This means that all the feedback loops are closed at the same time. Therefore, a better performance is achieved compared to the classical approach in which the control gains are selected individually. This quick and direct modern control approach can be utilized for time varying and time invariant systems, whereas the classical approach is mainly for time invariant systems. Also, there are many optimal control techniques that could be applied in the modern control theory to improve the controllability and stability of the UAV. However, not all states correspond directly to a single actuator, as was the case for the first approach. Therefore, it is difficult to handle actuator saturation. However, modern control

theory is also popular in hybrid UAVs as it was employed in Tilt-rotors, Tail-sitters and Ducted-Fans.

# CHAPTER 4

# AIRCRAFT DESIGN

## 4.1. MISSION REQUIREMENTS

Primary objective is to design the capital UAV that can lift as much as weight possible while adhering to the design specifications.

### 4.1.1. DESIGN SPECIFICATIONS

Initially we had fixed the following parameters for the design of Hybrid UAV.

Table 4.1. Design specifications

| Parameter | Value |
|---|---|
| Total Aircraft weight, *W* | 6 kg (with payload) |
| Payload Capacity | 1 kg |
| Cruise Velocity, | 15 m/s |
| Maximum height | 45 m |

### 4.1.2. FLIGHT PROFILE

For requirement purposes, the flight profile of the UAV is described next. Referring to Fig. 4.1, at position 'A' the FW-UAV will take-off vertically like a Quadrotor Drone (QD) and upon reaching a certain safe altitude 'B', the aircraft begins to hover. From this hovering position the UAV will fly forward like a usual fixed-wing aircraft, marked as position 'C'. The aircraft continues to fly forward and performs the assigned mission. Upon completion of the mission, the aircraft returns home or proceeds to a designated landing location, 'E'. This is done by forward flight first. As the aircraft approaches the landing location at some altitude, the airspeed slows down and the forward flight transitions to hover at an assigned altitude, marked here as position 'D'. Finally, FW-UAV descents vertically like a QD and completes the touch-down at position 'E'.

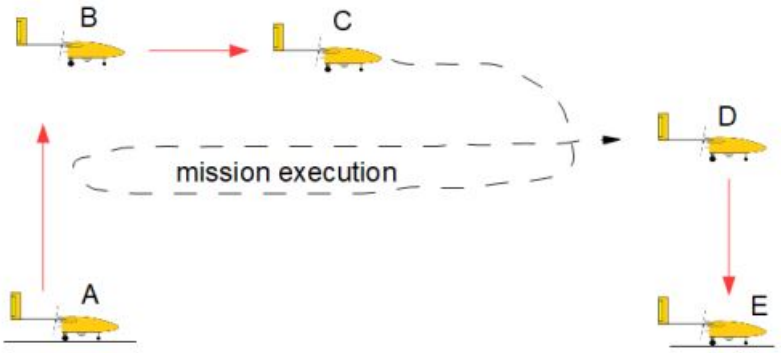


Fig. 4.1. Ideal Flight Plan and Profile of the designed UAV

## 4.2. AIRFOIL SELECTION

Wing is the crucial element in the design of a UAV. Wing design starts with the selection of the airfoil. The main objective of the process of airfoil selection is to determine the airfoil with maximum lift generation under the required operating conditions. Enhancing the lift produced is necessary to meet the objective of maximizing payload capacity. An enhanced lift equates to a higher payload capacity. A number of airfoils which comes under the category of high lift under low Reynolds number were chosen for comparison from the UIUC airfoil database with the help of airfoiltools.com [31].

Factors considered for comparison:

- Maximum lift coefficient
- Max $C_L/C_D$ ratio
- Pitching moment coefficient
- Stall angle
- Amount of travel of COP over a range of alpha

The airfoils selected for comparison (at Re = 2,00,000) were:

i. GOE226
ii. CH10
iii. MH60
iv. Clark-Y

### 4.2.1. AIRFOIL ANALYSIS, LIFT & DRAG REPRESENTATIONS

Considering the given available power plant & dimensional constraints of the UAV, the design lift coefficient was selected to be 1.1787. From among the listed airfoils, the one with the maximum $C_L/C_D$ ratio for the desired operating conditions was chosen as the primary airfoil for the UAV.

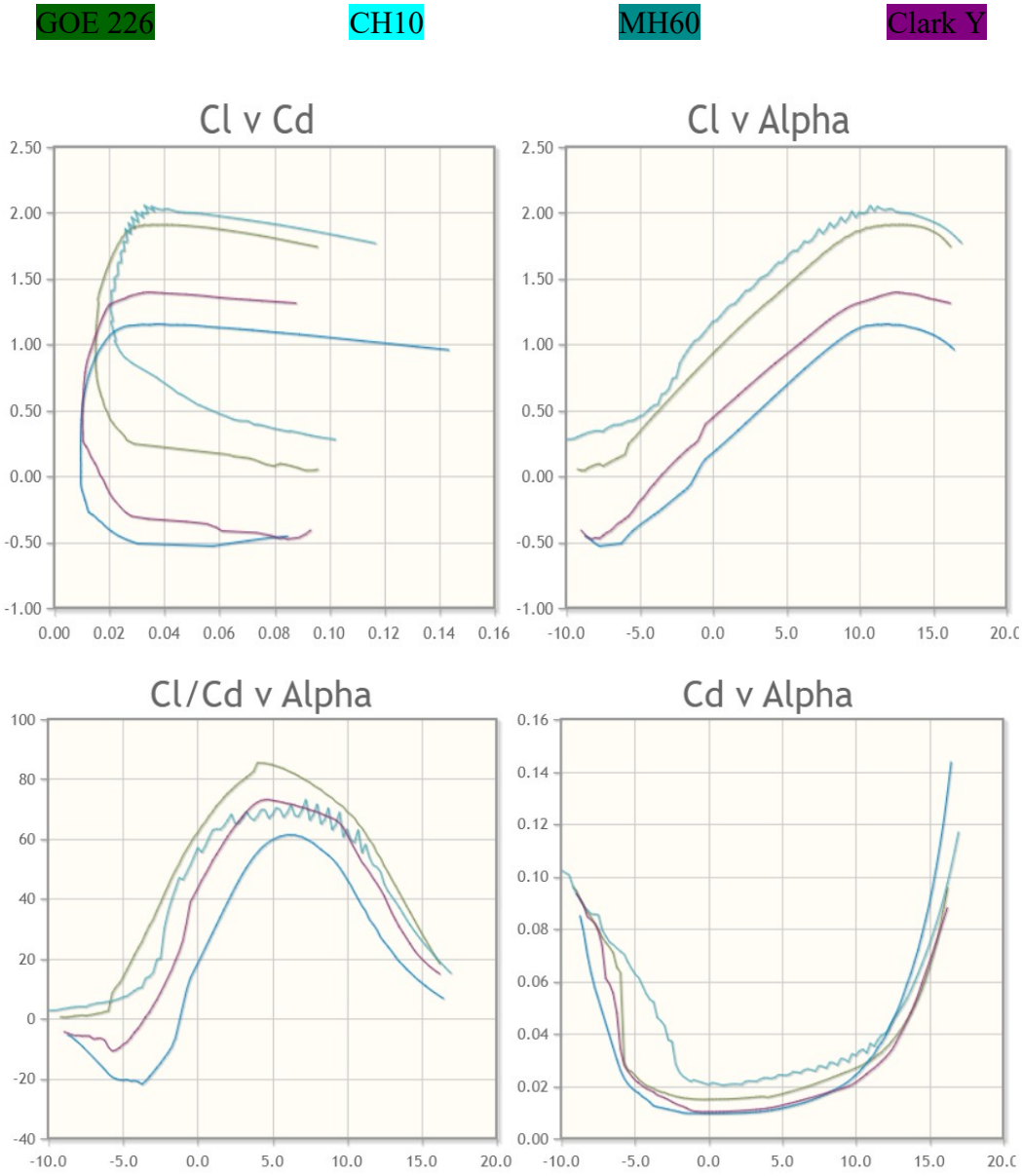


Fig. 4.2. Airfoil Comparison between GOE 226, CH10SM-IL, MH60-IL, Clark Y

A batch analysis of the 2-D wing was setup on XFLR5 analyzing the lift coefficient, drag coefficient, moment coefficient for varying angle of attack and Reynolds number for laminar flow. It was concluded that GOE 226 airfoil is best suited for payload lifting applications at a lower Reynolds number. It has the highest $C_L$ value at zero angle of attack which is required

for high payloads and also it has maximum lift coefficient. The profile of the selected airfoil is shown in Fig. 4.3.

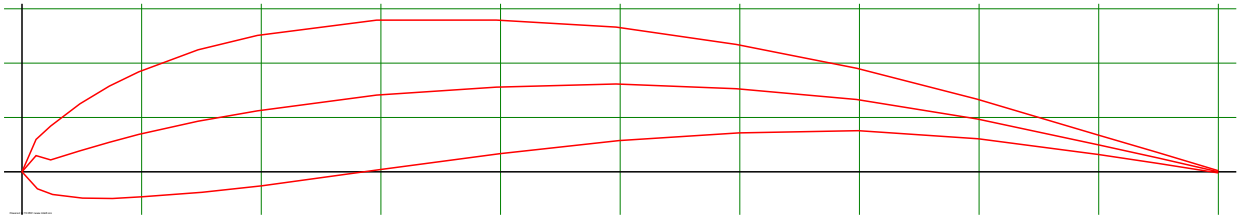

Fig. 4.3. Profile of GOE 226

## 4.3. WING DESIGN

The maximum value of $C_L$ for the given airfoil GOE226 is 1.9140. This value is the 2D lift coefficient $C_{L\max}$, i.e., the coefficient of lift for a wing of infinite span. When a wing of a finite span is considered, various end effects like induced drag, et cetera occur, which in turn, reduces the effective $C_L$ of the wing. The coefficient of lift of a finite wing can be found by using Prandtl's lifting line theory, which predicts the lift distribution over a three-dimensional wing, based on its geometry.

$$C_L = 0.8 \times CL_{max} \tag{4.1}$$

Therefore,

$$C_L = 1.5312$$

Table 4.2. Airfoil summary

| $\alpha$ | $C_L$ | $C_D$ | $C_M$ |
|---|---|---|---|
| 12.75 | 1.914 ($C_{Lmax}$) | 0.03743 | 0.0315 |
| 2.25 | 1.1787 (Design $C_L$) | 0.01537 | -0.2011 |

### 4.3.1. NUMBER OF WINGS

A single wing or monoplane is almost the only practical option in conventional modern aircraft. Owing to ease of assembly a single wing aircraft configuration is used as shown in Fig. 4.4.

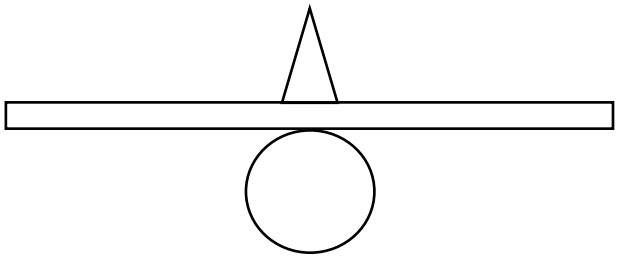

Fig. 4.4. Monoplane

### 4.3.2. WING VERTICAL LOCATION

One of the wing parameters that could be determined at the early stages of wing design process is the wing vertical location relative to the fuselage centerline. The high wing configuration was selected for the purpose of this project as it could create more lift compared to mid and low wing configurations. High wing will increase the dihedral effect ($C_{l\beta}$). It makes the aircraft laterally more stable. The reason lies in the higher contribution of the fuselage to the wing dihedral effect ($C_{l\beta}$). Other reasons include:

- Aerodynamically better span wise lift distribution
- Improved structural integrity and strength
- Can provide more room for payload
- Can facilitate easy handling of payload as well as service of aircraft
- Landing in remote places can be more safe
- Image capturing is not obstructed by any of the aircraft components
- Improved lift and CL values, low stall speed can be achieved.

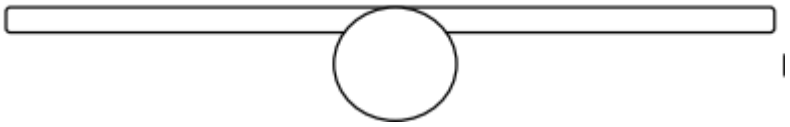

Fig. 4.5. High Wing

### 4.3.3. LIFT & DRAG CALCULATIONS

The total aircraft weight was fixed as 6 kg with payload and the cruise velocity was set as 15m/s (54kmph). A wing loading (W/S) of 150N/m$^2$ was chosen for the UAV. This was done to strike a balance between power required for maximum speed and battery weight needed for the endurance.

$$\frac{W}{S} = 150\ N/m^2$$

$$S = 9.81 \times \frac{6}{150} = 0.3924\ m^2$$

#### 4.3.3.1. ASPECT RATIO

Aspect ratio (AR) is defined as the ratio between the wing span (b) to the wing Mean Aerodynamic Chord (MAC or C). From historical data available, AR between 7 and 9 was selected for the fixed wing mode which is a preferred choice for Fixed wing RC Aircrafts.

$$\text{AR} = \frac{b}{C} \quad (4.2)$$

The wing planform area with a *rectangular or straight tapered* shape, is defined as the span times the mean aerodynamic chord:

$$S = b \times C \quad (4.3)$$

Chord length, $b = 0.23\ m$

Wingspan $C = 1.67\ m$

Therefore, Aspect Ratio $\text{AR} = \frac{b}{C} = 7.2:1$

### 4.3.3.2. CALCULATION OF REYNOLDS NUMBER

The airfoils chosen for comparison is taken at low Reynolds number (Re = 2,00,000) for higher lift. For verification, we calculated the Re for the wing with the chord length finally selected.

$$Re = \frac{\rho v c}{\mu} = 2{,}14{,}807$$

### 4.3.3.3. LIFT

The aircraft lift was calculated from the below equation:

$$L = \frac{1}{2}\rho v^2 S C_l \quad (4.4)$$

Lift, $L = \mathbf{58.86}\ N$

### 4.3.3.4. DRAG

The aircraft drag force was calculated from the below equation:

$$D = \frac{1}{2}\rho v^2 S C_D \quad (4.5)$$

Drag $D = \mathbf{0.767}\ N$

### 4.3.4. REQUIRED THRUST

From historical data, the required thrust to weight ratio (T/W) was assumed to be 0.55.

$$T/W = 0.55$$

So, required thrust $= \mathbf{32.373}\ N$

### 4.3.5. WING STRUCTURE

The structure of the wing will consist of

- Form-giving ribs and nose ribs.
- Longitudinal spars to pick up the bending forces.
- Skin to help carry the load during the vertical flight

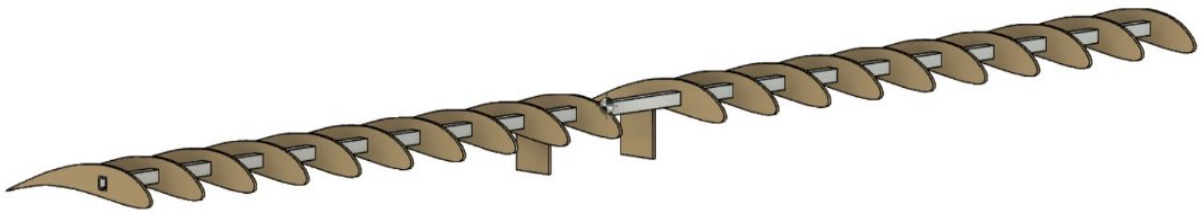

Fig. 4.6. Wing Skeleton

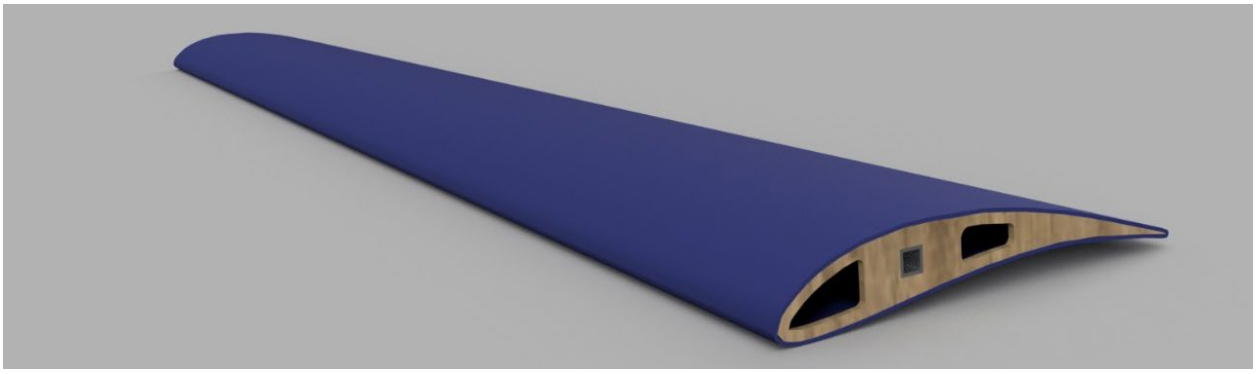

Fig. 4.7. Wing (Rendered image)

## 4.4. EMPENNAGE

Tail surfaces improve the overall aircraft stability and provide control surfaces for its pitch and yaw motion. Special attention was given while designing these surfaces as they add to the wetted area and also to the structural weight of the aircraft. The main purpose of stabilizers is to keep the aircraft in straight and level flight. For the horizontal and vertical stabilizer, a symmetrical airfoil NACA 0012 was selected.

### 4.4.1. HORIZONTAL STABILIZER

From historical data, area of horizontal stabilizer was taken as 20% of wing area,

Area of horizontal stabilizer, $S_H = 20\%\ of\ S_w$

$$S_H = 0.07682 m^2$$

*Horizontal Tail Volume Coefficient,* $C_H$*:* $(0.3 - 0.9)$

Taking $C_H = 0.9$

$$C_H = \frac{S_H \times L_H}{S_w \times b} \quad (4.6)$$

From equation (4.5), lever arm from the aerodynamic center of the wing to the aerodynamic center of the horizontal stabilizer, $L_H$ was found.

Horizontal Tail Moment Arm $L_H = \mathbf{1.035}\ m$

Taking, Aspect Ratio for the Horizontal Stabilizer,

$$AR_H = 1.6$$

Therefore, from the above considerations, the parameters for the Horizontal Stabilizer were selected as

Span, $\boldsymbol{b} = \mathbf{0.3506\ m}$

Chord, $\boldsymbol{C} = \mathbf{0.2191176\ m}$

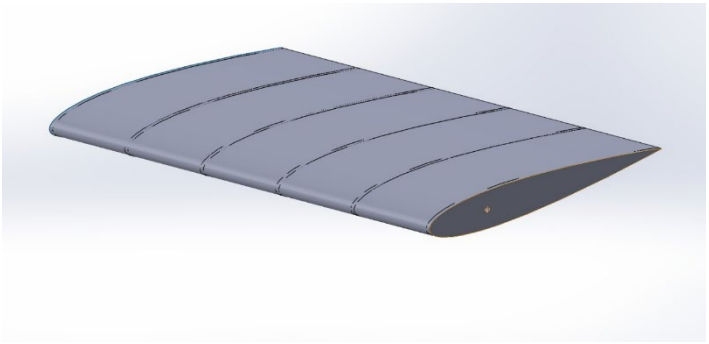

Fig. 4.8. Horizontal Stabilizer – CAD

### 4.4.2. VERTICAL STABILIZER

The vertical stabilizer maintains the lateral stability of the aircraft. From historical data, area of vertical stabilizer was taken as 8% of horizontal stabilizer area.

$Vertical\ Tail\ Volume\ Coeff.,\ C_v: (0.02\ -0.05)$

From Historical Data,

Area of vertical stabilizer, $S_V = 8\%\ of\ S_w$

$$S_V = 0.030728\ m^2$$

$$C_V = \frac{S_V \times L_V}{S_w \times b} \tag{4.7}$$

Taking $C_V = 0.05$

From equation (4.6), lever arm from the aerodynamic center of the wing to the aerodynamic center of the vertical stabilizer, $L_v$ was found.

Vertical Tail Moment Arm $L_V = \mathbf{1.04375}\ m$

$$AR_V = 1.6$$

Therefore, from the above considerations, the parameters for the Vertical Stabilizer were selected as

Span, $\boldsymbol{b = 0.22173\ m}$

Chord, $\boldsymbol{C = 0.138583\ m}$

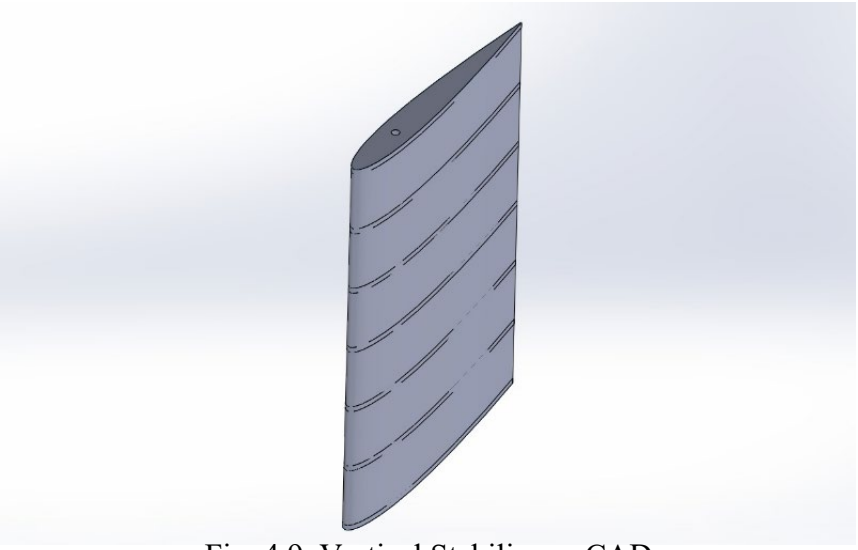

Fig. 4.9. Vertical Stabilizer – CAD

## 4.5. STABILITY CALCULATIONS

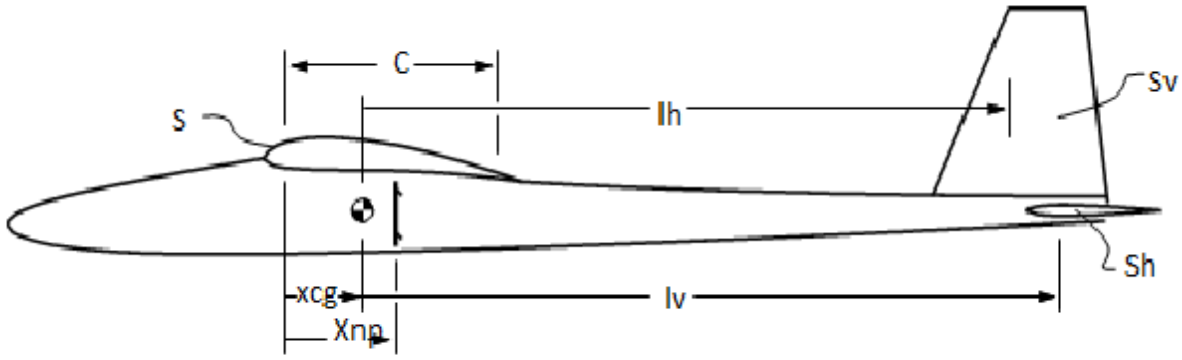


Fig. 4.10. Critical points for stability

### 4.5.1. NEUTRAL POINT

Neutral point is the position of center of mass at which the aircraft would be neutrally stable. If the center of mass is behind of this point, it results in an unstable aircraft that will increasingly turn with any manoeuvre the pilot makes

$$\frac{x_{np}}{c} = \frac{1}{4} + \frac{1+\frac{2}{AR}}{1+\frac{2}{AR_H}}\left(1-\frac{4}{AR+2}\right)C_H \qquad (4.8)$$

Therefore, the position of neutral point from the leading edge from equation (4.7) is $x_{np}$.

$$\therefore, \boldsymbol{x_{np}} = \boldsymbol{0.12394\ m}$$

### 4.5.2. STABILITY MARGIN

The stability margin is used to calculate the position of center of gravity from the leading edge of the wing.

$$S.M. = \frac{x_{np}-x_{cg}}{c} \qquad (4.9)$$

Taking $S.M. = 0.1$

$$\therefore, \boldsymbol{x_{cg}} = \boldsymbol{0.10094\ m}$$

### 4.5.3. AERODYNAMIC CENTER

In the normal flight range, the resultant aerodynamic forces acting on any lifting surface (e.g. lift, tail) can be represented as a lift and drag acting at the Aerodynamic Center (ac), together with a pitching moment which is independent of angle of attack. The aerodynamic center lies in the plane of symmetry of the wing.

According to Thin Airfoil Theory, A.C. is exactly at ¼th Chord for symmetrical airfoils & slightly less than ¼th Chord for cambered airfoils.

$$\therefore, x_{ac} = 0.0575m$$

Distance between nose and leading edge of the wing is fixed as **16cm**.

| | |
|---|---|
| ∴, distance between nose and centre of gravity, | $l_{cg} = 26.094\ cm$ |
| Distance between nose and aerodynamic centre, | $l_{ac} = 21.75\ cm$ |
| Distance between nose and neutral point, | $l_{np} = 28.394\ cm$ |

## 4.6. VTOL MODE DESIGN

Since the project is being concentrated to have vertical take-off capabilities, a Quad-rotor/Quadcopter Configuration is implemented in the aircraft system. Quadcopters use 2 sets of identical fixed pitch propellers; 2 clockwise (CW) and 2 counter-clockwise (CCW). These use variation of RPM to control lift and torque. Control of vehicle motion is achieved by altering the rotation rate of one or more rotor discs, thereby changing its torque load and thrust/lift characteristics.

### 4.6.1. FORCES AND TORQUE ACTING ON THE QUAD-ROTOR CONFIGURATION

A quadcopter in full motion experiences the following forces and toque [32] acting upon it:

a) Lift generated by each motor.
b) Gravitational pull acting on total lift generated
c) Yaw, roll and pitch movements can be achieved by generating moments in the respective axes
d) Yawing torque is the resultant of the four individual torques generated by propellers
e) Rolling torque can be produced by increasing left motor's thrust and decreasing right motor's thrust and vice-versa
f) Pitching torque can be generated by increasing front motor's thrust and decreasing back motor's thrust and vice-versa

The above mentioned forces and torques acting upon the FW VTOL aircraft are chiefly responsible for lifting the aircraft into the air and providing further stability to the aircraft at high altitude levels. It basically increases the manoeuvrability of the aircraft to hover at the required conditions without losing its stability at any cost whatsoever. As mentioned above, the yawing torque is provided by the resultant of the four individual torques acting upon the system, the rolling torque is due to the difference between the thrust produced by the left and right motors and the pitching torque is caused due to the difference between the thrust produced by the front and back motors. Lift and gravitational forces apply forces upon the aircraft in two opposite directions i.e., upward and downward.

The assumed Thrust-to-Weight ratio for the aircraft for VTOL mode is 2:1.

$$T/W = 2$$

Thrust produced by each motor, $T_{individual}$

$$T_{individual} = \frac{2 \times Weight\ of\ the\ aircraft}{4} \tag{4.10}$$

Therefore, each motor is required to produce a maximum thrust of 29.43 N. The required propulsion and power plant system has been discussed in Chapter 5.

### 4.6.2. QUADROTOR DYNAMICS

As discussed above, the Quadrotor flight mode has four control inputs [33]—throttle, roll, pitch and yaw. The throttle input is used to climb or descend. The roll input tilts the UAV to make it move sideways. Pitch input tilts the UAV up or down. Yaw input rotate the UAV around its axis. In order to perform these four motions using throttle, roll, pitch, and yaw commands, the propeller speeds are adjusted as shown in Fig. 1.1.

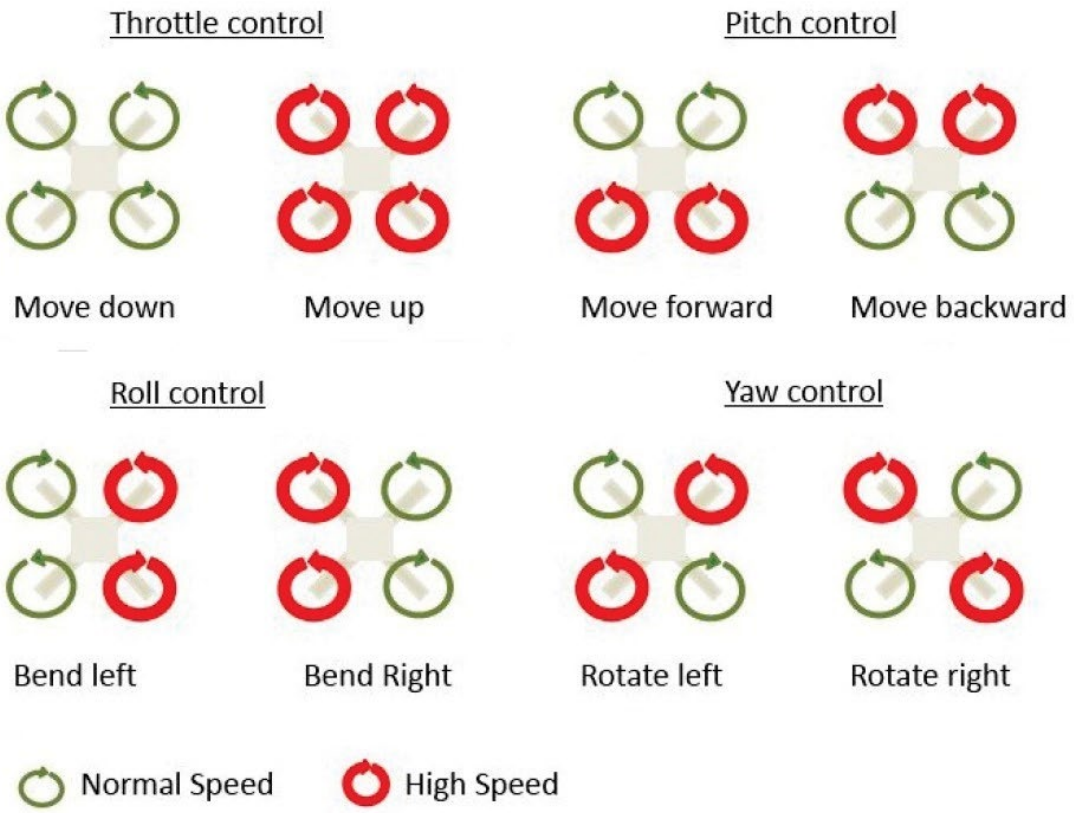


Fig. 4.11. Propeller speeds in throttle, roll, pitch and yaw control

Detailed discussion about the motion of the aircraft is given in Chapter 9.

# CHAPTER 5

# SIZING OF POWER PLANT

A nose mounted, electric driven motor-propeller combination constitutes the primary components of power plant for the fixed-wing mode. An electric propeller was chosen to reduce weight while satisfying the endurance requirement. For the quadrotor mode, suitable motor-ESC combinations are selected with considerations on thermal effects and battery drainage. The power and KV rating of motor required was calculated based on the mission requirements. Suitable calculations [34], [35] to estimate the endurance and range has been made.

## 5.1. POWER REQUIRED FOR FIXED-WING MODE

From the literature analysis [34], we made following conclusions:

- For power required to be minimum, $C_L^{\frac{3}{2}}/C_D$ should be maximum.
- The airplane needs to be flown at $C_L$ such that $C_L^{\frac{3}{2}}/C_D$ is maximum.
- The airplane needs to have sufficient speed so that the lift produced by the aircraft at $C_L$ corresponding to $C_L$ for $\left[C_L^{\frac{3}{2}}/C_D\right]_{max}$ is able to balance the weight of the aircraft.

Power required ($P_{req}$):

$$P_{req} = \frac{1}{2}\rho V^3 S C_{D_0} + \frac{\left(\frac{W^2}{\frac{1}{2}\rho V S}\right)}{\pi A R e} \quad (5.1)$$

$$P_{req} = 64.4\ W$$

### 5.1.1. RPM CALCULATION

The size designation of all propellers is comprised of two basic measurements: diameter and pitch. The measurement for pitch does not pertain to a physical measurement of the propeller itself, but rather it indicates the distance of forward travel per revolution of the propeller in inches. The following relation was used to select a suitable motor with desired RPM:

$$\frac{RPM \times pitch}{1056} = speed\ in\ mph \quad (5.2)$$

$$RPM \times pitch = 1056 \times 33.554$$

A propeller pitch of 8” was selected to keep the RPM less than 9000, as most of the BLDC motors have a maximum of 9000 RPM.

*Minimum required RPM* = 4429.128

### 5.1.2. KV CONSTANT OF MOTOR

KV is not a rating, but rather a motor constant. It tells us about how the generated back-emf in the motor relates to motor speed. The formula to calculate KV for brushless motors is:

$$KV = \frac{RPM}{Volts \times 1.414 \times 0.95} \tag{5.3}$$

This is just speed divided by voltage, but the ‘1.414’ term is to convert RMS voltage to peak voltage. The ‘0.95’ term is the fudge factor. Nominal voltage of selected battery is 22.2 V. So required KV constant is 200. Subject to availability in market, 220 KV motor is selected.

### 5.1.3. ENDURANCE

The maximum endurance of an aircraft (or the time aloft) refers to a flight condition that requires the minimum fuel power [36]. Thus, the minimum power (maximum endurance) condition occurs at a speed which is 76% of the minimum drag (maximum range) condition. The corresponding lift-to-drag ratio is 86.6% of the maximum lift-to-drag ratio. Energy required for 1hr endurance:

$$E_{1hr} = 1.1 \times \sqrt{\frac{2W_0\frac{W}{S}}{\rho_{battery}\eta_m\eta_p\eta_{dis}f_{DoD}}} \times \left(0.25\left(\frac{3}{kC_{D_0}^{\frac{1}{3}}}\right)^{\frac{3}{4}}\right)^{-1} \tag{5.4}$$

$$E_{1hr} = 40.87\ Wh$$

Table 5.1. Power plant parameters

| | |
|---|---|
| Propeller efficiency, $\eta_p$ | 0.7 |
| Motor Efficiency, $\eta_m$ | 0.8 |
| Battery Discharge Efficiency, $\eta_{dis}$ | 0.95 |
| Depth of Discharge, $f_{DoD}$ | 0.9 |
| Battery Power density, , $\rho_{battery}$ | 192.28h/kg |

## 5.2. PROPULSION SYSTEM- QUADROTOR CONFIGURATION

Since total mass of the aircraft has been fixed to 6 kg, the required thrust produced by the four motors combined should be double the weight of the aircraft for effective control. Therefore, we have taken the thrust-to-weight ratio for achieving the VTOL capability as 2:1. So we had to select a suitable motor that could generate a thrust of 3 kg which when combined provide (3 x 4) kg thrust. Thus, the take-off capability is predetermined to be achieved at 50% throttle. BLDC motors of following specification: T-Motor MN 5212 420 KV is selected for the purpose. The propellers for the system are T-Motor 18 x 6.1 Carbon fiber. The bench test data has been provided by the manufacturer.

Now the required battery combination is to be selected for which we have preset the hovering flight time to 10 minutes. The current input required for above conditions is 49.6 A (12.4 A * 4 nos.). Required Battery Capacity = (time * Amps)/ 60

Required Battery Capacity = 4.96 Ah

## 5.3. SELECTION OF BATTERY

The effective battery Ah required is calculated assuming a minimum one hour flight endurance in FW mode, along with VTOL in quadrotor mode. Energy required for one hour endurance is obtained and converted to Ah. So total Ah, while considering the battery effectiveness to be 78%, is 11.12 Ah. A suitable LiPo battery: 12000 mAh and nominal voltage 22.2V is selected.

## 5.4. SUMMARY OF POWER PLANT

This section describes the specifications of the components used for propulsion in both FW mode and VTOL mode. The values have been taken from the specifications given by the manufacturer on the product.

### 5.4.1. FIXED WING MODE

#### 5.4.1.1. BLDC MOTOR SPECIFICATION (Model: T-Motor AT 3520 KV850 [37])

Table 5.2. KV850 BLDC parameters (Fixed Wing)

| Parameter/Power rating (KV) | Long Shaft KV850 |
|---|---|
| Motor Dimensions | Ø43*65mm |
| Shaft Diameter | IN : 10mm, OUT : 8mm |
| Idle Current (10V) | 1.8A |

| | |
|---|---|
| Max. Power (180s) | 2700W |
| Weight | 221g |
| Internal Resistance | 14mΩ |
| Configuration | 12N14P |
| Rated Voltage (Lipo) | 3-4S |
| Peak Current (180s) | 70A |


Fig 5.1. BLDC Motor for horizontal flight

#### 5.4.1.2. **ESC** (Model: T-Motor AT 75A 6S [38])

Table 5.3. 75A ESC parameters

| | |
|---|---|
| Parameter/ ESC rating(A) | 75 |
| Max continuous current (A) | 75 |
| Peak current (A) | 95 A for 10 s |
| BEC | 5V/5A |
| Size | 86*38*12 |
| Weight | 82 g |


Fig 5.2. 75A ESC

#### 5.4.1.3. **PROPELLER** (Model: APC 18x8E [39])

Table 5.4. APC 18x8 Propeller parameters

| | |
|---|---|
| Parameter/ Propeller | 18 x 8 |
| Pitch (in.) | 8 |
| Propeller diameter (in.) | 18 |

| | |
|---|---|
| Hub Diameter (in.) | 1.75 |
| Hub Thickness (in.) | 0.59 |
| Shaft Diameter (in.) | 5/16 in. |
| Weight | 130 g |
| Material | Carbon Fiber |

Fig 5.3. APC 18x8 propeller

### 5.4.2. VTOL MODE

#### 5.4.2.1. BLDC MOTOR SPECIFICATION (Model: T-Motor MN5212 KV420 [40])

Table 5.5. KV420 BLDC parameters (Quadrotor Configuration)

| Parameter/Power rating (KV) | Long Shaft KV220 |
|---|---|
| Motor Dimensions | Ø59*33.5mm |
| Shaft Diameter | 4 mm |
| Idle Current (10V) | 1.1A |
| Max. Power (180s) | 1440W |
| Weight | 249g |
| Internal Resistance | 69mΩ |
| Configuration | 24N22P |
| Rated Voltage (Lipo) | 4-8S |
| Peak Current (180s) | 60A |


Fig 5.4. BLDC Motor for VTOL

#### 5.4.2.2. **ESC** (Model: T-Motor ALPHA 60A 6S [41])

Table 5.6. 55A ESC parameters

| Parameter/ ESC rating(A) | 55 |
|---|---|
| Max continuous current (A) | 40 |
| Peak current (A) | 60 A for 10 s |
| BEC | 5V/5A |
| Size | 71*33*16 |
| Weight | 63 g |


Fig 5.5. ESC for VTOL Motors

#### 5.4.2.3. **PROPELLERS** (Model: T-Motor P18x6.1 [42])

Table 5.7. T-Motor 18x6.1 Propeller parameters

| Parameter/ Propeller | 18 x 6.1 |
|---|---|
| Pitch (in.) | 6.1 |
| Propeller diameter (in.) | 18 |
| Weight | 60 g |
| Material | Carbon Fiber + Epoxy |

Fig 5.6. 18x6.1 Propellers for VTOL motors

### 5.4.3. **BATTERY** (Model: GensTattu TA-25C-12000-6S1P-AS150 [43])

Table 5.8. LiPo parameters

| Parameter/battery (mAh) | 12000 mAh |
|---|---|
| Voltage (V) | 22.2 |
| Configuration | 6S1P |
| Nominal cell voltage(V) | 4.2 |
| Discharge rate (C) | 15 |
| Maximum discharge rate (C) | 50 |
| Connector type | AS150+XT150 |
| Weight (g) | 1400 g |


Fig 5.7. Lipo Battery 12000 mAh

## 5.5. RANGE

The range (R) of the aircraft has been theoretically calculated from the given equation:

$$R = E^* \frac{m_{batt}}{m} \frac{1}{g} \frac{L}{D} \eta_{total} \quad (5.5)$$

This equation is similar to the 'Breguet range equation', used for fossil fuel aircrafts. It shows the influence of aircraft, propulsion system, and structural design parameters. Here, $m_{batt}$ is the mass of the battery and m, the total mass of the aircraft. $E^*$ is battery specific energy that is determined from the data of the battery build. From estimation, the available $E^*$ is assumed as 1.86 Ah. L/D ratio is proportional to L/T ratio which is $(0.55)^{-1}$.

Therefore, the range calculated was **R = 4.9 km**, with the available propulsion system.

The power plant is chosen so that the system has sufficient energy to achieve a level flight, in addition to satisfying the vertical take-off, hovering, stabilizing and landing capability in quadplane mode. After consideration of such energy requirements, the range calculation for fixed-wing mode is made.

# CHAPTER 6

# ELECTRONICS AND CONTROL

The UAV requires sensors that observe the current state of the aircraft and record changes in its surroundings to achieve autonomy. There is a variety of hardware required to get this data, process it, and alter the aircraft state to finish the assigned mission. The following subsection gives the overview of the system.

## 6.1. HARDWARE

A Pixhawk PX4, depicted in Fig. 6.1, was selected as the flight controller for the autonomous system. *Pixhawk 4*® is an advanced autopilot designed and made in collaboration with Holybro® and the PX4 team. It is optimized to run PX4 v1.7 and later, and is suitable for academic and commercial developers.


Fig. 6.1. Pixhawk 4 *(source: www.pixhawk.org)*

A typical autopilot wiring connection [44], as shown in Fig. 6.2., has been used for the purpose of the project.

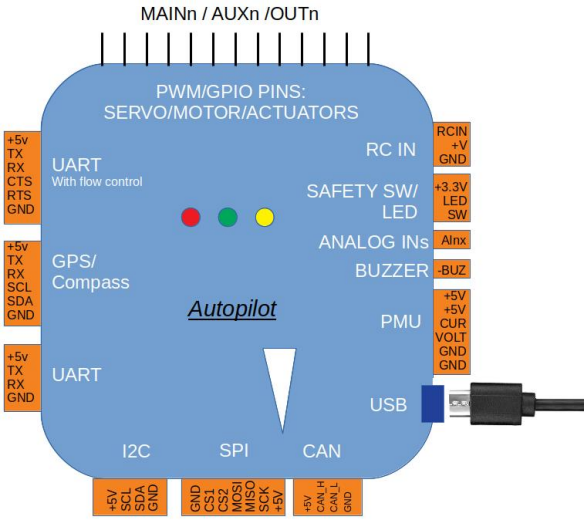


Fig. 6.2. Wiring Connection for PX4 (*source: www.ardupilot.org*)

On board the aircraft, a GPS and telemetry unit has to be installed. The GPS device reads the position, speed and altitude of the UAV. This data, along with information on battery status and sensor data, could be sent back to the ground centre via the telemetry unit. Radio Control receivers are normally used for pilot control.

A schematic of the full setup for the VTOL-UAV project, depicting the flight controller unit, telemetry & GPS unit, receiver, battery and ESC-BLDC motor configurations, is shown in Fig. 6.3.

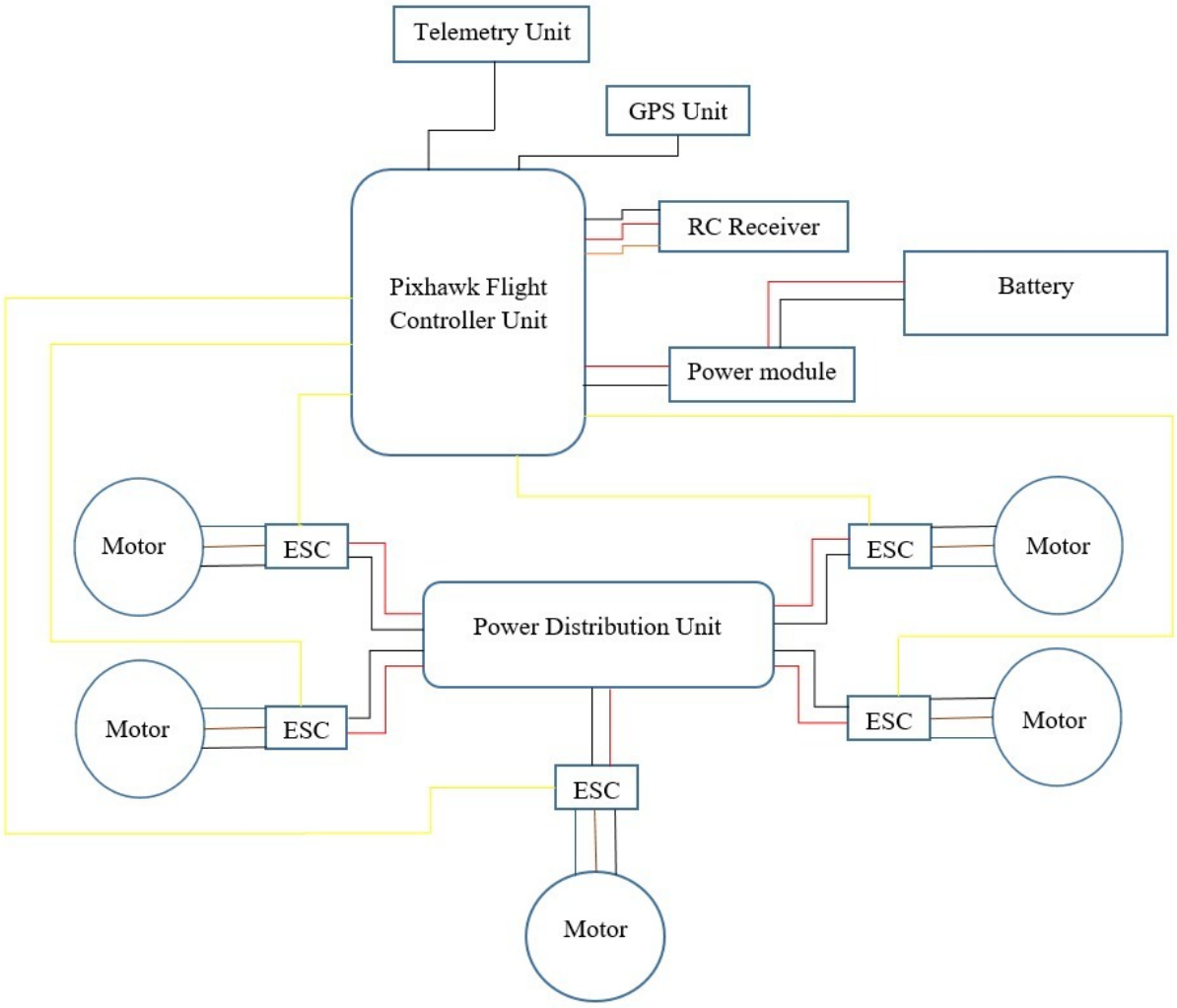


Fig. 6.3. Schematic of the Hardware connections

## 6.2. SOFTWARE

The basic software structure of the aircraft can be represented in five levels:

1. **User Interface / Application Programming Interface (UI / API):** A User Interface and Application Programming Interface is a software layer that provides a user-friendly tool set and options to implement waypoint guidance, geofencing, sensor calibration,

and to program the companion computer. An API also gives a mode to connect the companion computer with the flight controller. For this project, Mission Planner: Ardupilot was selected.

2. **Communication Layer:** The communication layer is used to establish communication between the UI/API and the flight controller. Depending on the application, this communication can be wired or wireless. Wired communication is usually implemented through USB. Wireless communication is dictated by the range of communication required. For a range less than 10 km, WiFi connection and radio telemetry is used. Application with range larger than 10 km uses cellular connection or long-range radio telemetry kits [44].
3. **Flight Code:** Flight code is further divided into three main layers:
    a. **Vehicle code:** Flight code is specific to a type of aircraft. In this project, Arduplane, a plane variant of ArduPilot firmware, is used on this level of the software system. Since Arduplane firmware gives a further option of specifying an aircraft configuration, the Quad Plane flight configuration code [45] was used for this project with necessary editing done for achieving the flight profile and for configuring with ESCs and BLDC motors used. The specific vehicle code is indexed in the Appendix 1.1 with the link to the repository in the team's Github page.
    b. **Libraries:** Libraries were used to reduce the number of programs that had to be written from scratch. These libraries include sensor drivers, attitude and position estimation (Extended Kalman Filters)[44].
    c. **Hardware Abstraction Layer (HAL):** The Hardware Abstraction Layer is a set of libraries for interfacing with different flight controllers in the market, for example Pixhawk, ArduPilot Mega, and Snapdragon Flight Controller. This increases the number of compatible flight controllers with the choice of firmware.
4. **Real-Time Operating System (RTOS):** Since Pixhawk PX4 was selected for this project, a PX4 firmware, inbuilt in the Arduplane firmware, is used to interface with the Pixhawk. This PX4 firmware is built on a real-time operating system called NuttX.
5. **Hardware:** The hardware level of the system specifies the hardware that will be used in the system. This hardware level is discussed in the Section 6.1.

## 6.3. COMMUNICATION

The aircraft's communication systems are responsible for the numerous hardware and software components of the quadplane to work in harmony. Communication systems allow the quadplane and its operator to achieve specific tasks during operational flight. Without successful communication systems, not only the unmanned flight but also the data transfer within the system required for autonomous navigation would be impossible.

The telemetry radio kit includes two antennas that act as both a transmitter and a receiver. One of these two antennas should be used at each communication point, the Pixhawk and the Ground Control Station.

The hand-held transmitter uses AFHDS 2A protocol to communicate with the aircraft using a receiver. To establish this protocol, a Flysky FS-i6 transmitter and an AR receiver that supports AFHDS protocol could be used. This transmitter uses 2.4 GHz frequency for communications.

The wired communication system is responsible for relaying information between Pixhawk and peripheral sensors and GPS. MAVLink is a communication protocol that communicates data between two nodes regardless of the underlying physical communication interface used. For physical communication interfacing, the serial connection could be established using the "Telem 2" serial port on Pixhawk.

## 6.4. FLIGHT CONTROL

To achieve autonomous flight, the aircraft has to switch between quadrotor mode and FW mode. The ArduPlane firmware have this feature inbuilt in form of Quad-Plane configuration code [44]. This code was enabled by setting the QENABLE parameter in Mission Planner to 1 (QENABLE=1). Enabling the code gives access to flight modes that allowed the quadrotor and FW characteristics to coexist and transition between them. Using the transmitter, it is possible to switch between flight modes manually. Several of the flight modes that is used are listed below.

1. QSTABILIZE: Stabilizes the aircraft around the roll and pitch axis.
2. QHOVER: Maintains the altitude of the aircraft while hovering.
3. QLOITER: Maintains the aircraft's altitude while circling around a given position.
4. QLAND: Lands the aircraft using VTOL in a desired location.
5. FBWA (Fly-By-Wire A): Assists in flying in Fixed Wing mode. For this mission this mode would be used to transition to and perform horizontal flight.

# CHAPTER 7

# STRUCTURAL ANALYSIS OF WING

In this this section, the design of Hybrid UAV using CAD software is discussed. In addition, the structural analysis performed for the wing has also been included.

## 7.1. CAD

For design of various components in the aircraft structure, Solidworks® software was primarily employed along with Autodesk Fusion 360 for cloud utility. The standard parts were derived from McMaster Carr components [46]. Detailed discussion on the materials selected has been given in Chapter 8.

### 7.1.1. AIRCRAFT WING

The aircraft wing consists of:

- Form-giving ribs
- Longitudinal spar to pick up the bending forces.
- Skin to help carry the load during the vertical flight

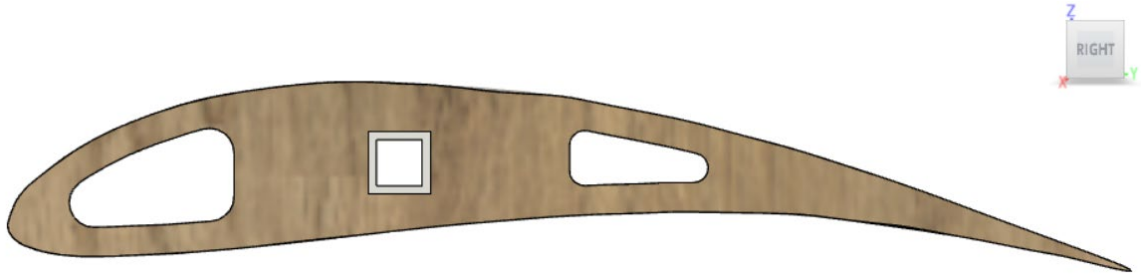


Fig. 7.1. Side view of the wing rib (GOE226 profile)

Fig. 7.2. Wing skeleton

### 7.1.2. QUADPLANE FRAME

For the ease of assembly and manufacture for the particular aircraft configuration, H frame was selected for assembling BLDCs for VTOL. M7.5 bolts and nuts are used for attachment of the square section spars.

Fig. 7.3. H frame

Fig. 7.4. H frame with BLDC and Propeller assembly

### 7.1.3. EMPENNAGE

T- Tail configuration has been selected for the empennage design with symmetric airfoil NACA 0012. The geometry of spars for both the horizontal and vertical stabilizers are cylindrical.

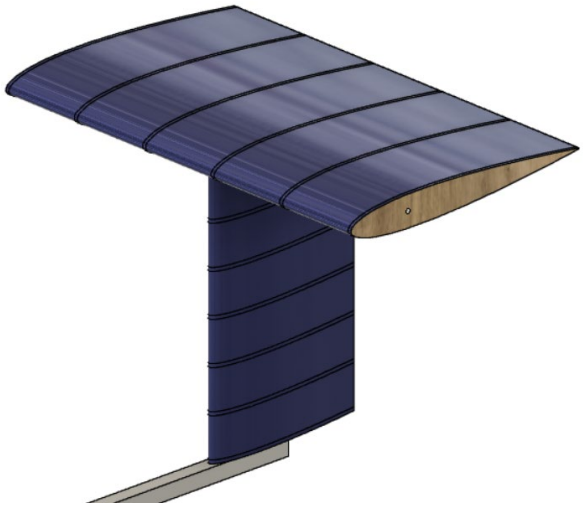

Fig. 7.5. Aircraft tail

### 7.1.4. HORIZONTAL MOTOR ASSEMBLY

We used a standard model for the BLDC motor, available from GrabCAD. M3 bolts have been used for attachment to the nose.

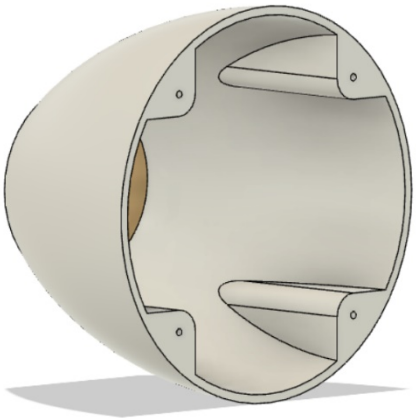

Fig. 7.6. Aircraft nose

Fig. 7.7. Horizontal Motor Assembly

### 7.1.5. FUSELAGE

Aircraft fuselage includes the space to equip battery, flight controller, ESCs and payload. A custom battery-&-flight-controller holder has been designed for the project's purpose. Also, a 150*80*80 mm payload bay has been included for initial flight tests, which can be improved by redesigning it after the tests. The position of flight controller is such that the arrow head point towards propeller tip.

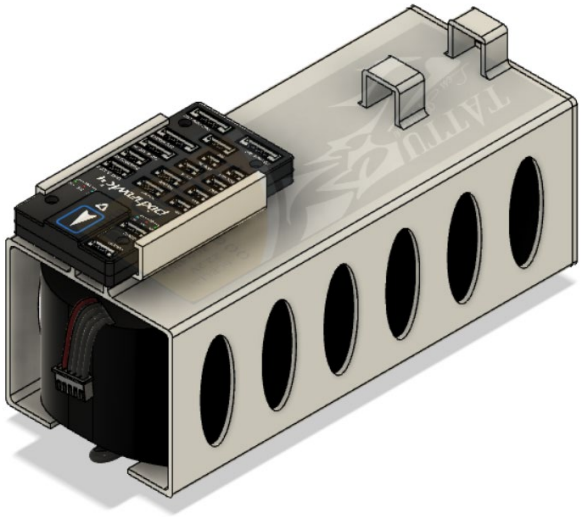

Fig. 7.8. Battery & Flight Controller holder

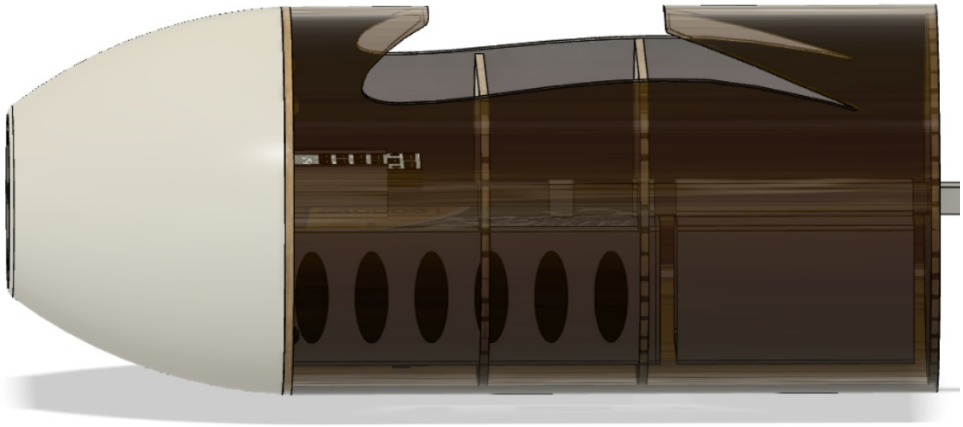

Fig. 7.9. Fuselage

### 7.1.6. FULL ASSEMBLY

The full assembly of the system has been shown in Fig. 7.11. This section also shows an evolution of the CAD design adopted for the project from initial stage to final model.

Fig. 7.10. Initial design

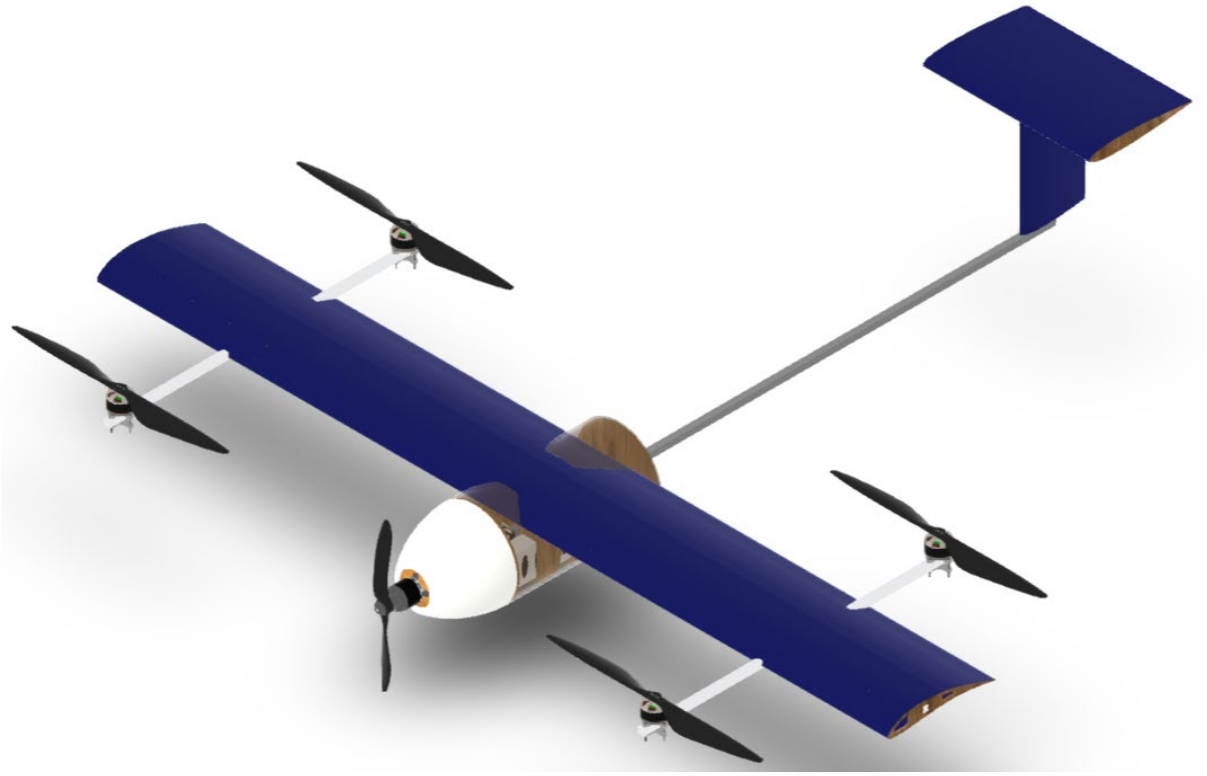

Fig. 7.11. Final CAD Assembly

The links to the project CAD files has been included in Appendix 1.2.

## 7.2. INFERENCE FROM CAD

This section includes some crucial inferences derived from the CAD model, that is used in the simulation part such as projected area and moment of inertia along the X, Y and Z axes.

### 7.2.1. PROJECTED AREA

a) The projected area in x-direction is denoted as $A_x$

| | | |
|---|---|---|
| Area of Struts | = | $15679.42\ mm^2$ |
| Area of Airfoil Profile of the wing | = | $4476.22\ mm^2$ |
| Central stem projected area | = | $13538.7\ mm^2$ |
| Area of Fuselage | = | $69160\ mm^2$ |
| Projected area of Horizontal & Vertical Stabilizer | = | $34674.37\ mm^2$ |
| Projected area of Nose | = | $26010\ mm^2$ |
| Total Area, $A_x$ | = | $163598.01\ mm^2 = 0.1635\ m^2$ |

Including the area of propellers, motors, etc.

$$\therefore \boldsymbol{A_x} \approx \mathbf{0.184\ m^2}$$

b) The projected area in y-direction is denoted as $A_y$

| | | |
|---|---|---|
| Area of Struts | = | $7620\ mm^2$ |
| Area of wing | = | $63460\ mm^2$ |
| Area of Fuselage | = | $67600\ mm^2$ |
| Projected area of Horizontal & Vertical Stabilizer | = | $11065.86\ mm^2$ |
| Total Area, $A_y$ | = | $149745.86\ mm^2 = 0.1497\ m^2$ |

Including the area of propellers, motors, etc.

$$\therefore \boldsymbol{A_y} \approx \mathbf{0.17\ m^2}$$

c) The projected area in z-direction is denoted as $A_z$

| | | |
|---|---|---|
| Area of Struts | = | $9720.58\ mm^2$ |
| Area of Wing | = | $384100\ mm^2$ |
| Area of Central stem | = | $12509.7\ mm^2$ |
| Area of Fuselage (not covered by wing) | = | $7060\ mm^2$ |
| Projected area of Horizontal Stabilizer | = | $76911.12\ mm^2$ |
| Area of Nose | = | $26010\ mm^2$ |
| Total Area, $A_z$ | = | $516311.4\ mm^2 = 0.5163\ m^2$ |

Including the area of propellers, motors, etc.

$$\therefore \boldsymbol{A_z} \approx \mathbf{0.63\ m^2}$$

### 7.2.2. MOMENT OF INERTIA

Moments of inertia at the center of mass, considering aircraft mass to be 6 kg, along X, Y and Z directions are denoted as $I_x$, $I_y$ and $I_z$ respectively.

Along x-direction, $\boldsymbol{I_x} = \ 671234581.85\ g.mm^2 = \ \mathbf{0.6712\ kg.m^2}$

Along y-direction, $\boldsymbol{I_y} = \ 1194368874.48\ g.mm^2 = \ \mathbf{0.11944\ kg.m^2}$

Along z-direction, $\boldsymbol{I_z} = \ 1799457067.74\ g.mm^2 = \ \mathbf{0.1799\ kg.m^2}$

## 7.3. ANALYSIS

### 7.3.1. INTRODUCTION

The wing is a primary structural component of an aircraft which is used to produce lift force during flight. Wing must have high strength to weight ratio and high fatigue life since it is subjected to alternate repeated loadings during flight. The main aim in doing the stress analysis is to check whether the chosen material has enough strength to withstand the lift force generated. The software used is Fusion 360.

### 7.3.2. MATERIAL SELECTED

In this study, aircraft wing structure with skin, spars and ribs is considered for the detailed analysis. The wing structure consists of 18 ribs and one spar with skin. The selected material for spar is Aluminum 7075 and birch wood for ribs. Their material properties are given in Table 7.1.

Table 7.1 Material properties

| **Material** | **Aluminum** | **Birch wood** |
|---|---|---|
| Density | 2.81E-06 kg/mm$^3$ | 5.12E-07 kg/mm$^3$ |
| Young's Modulus | 71.7 GPa | 13.86 GPa |
| Poisson's Ratio | 0.33 | 1E-04 |
| Yield Strength | 145 MPa | 1E-05 MPa |
| Ultimate Tensile Strength | 276 MPa | 1E-05 MPa |
| Thermal conductivity | 0.173 W/(mmC) | 1.8E-04 W/(mmC) |

### 7.3.3. BOUNDARY CONDITIONS

The loads and boundary conditions along with meshed model are shown in Fig 7.12 and Fig 7.13. below. One end of the wing is fixed since it is embedded inside the fuselage and other end is left free. Pressure force of 550 Pa is applied at the bottom surface of the wing at center of pressure. Center of pressure is a point at which total pressure is assumed to be act [47].

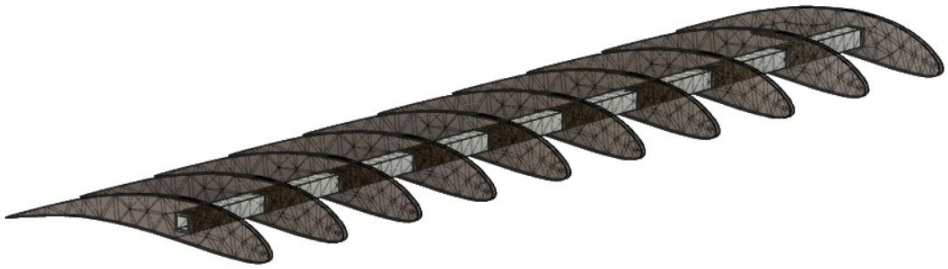

Fig. 7.12. Meshed Left half wing

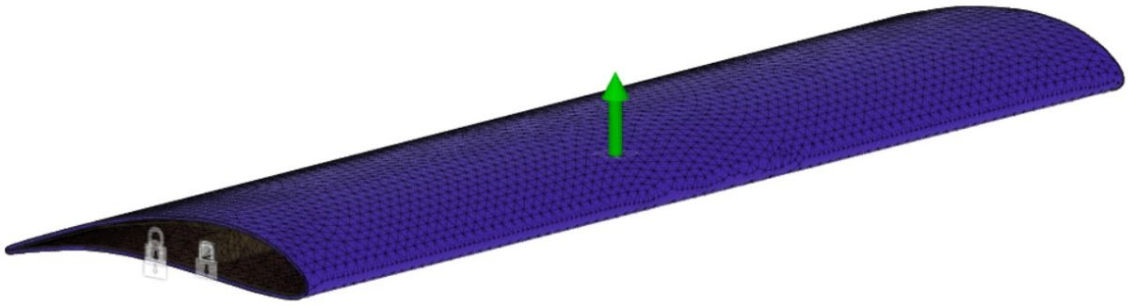

Fig. 7.13. Boundary conditions

### 7.3.4. STATIC STRUCTURAL ANALYSIS RESULTS


Fig. 7.14. Maximum displacement

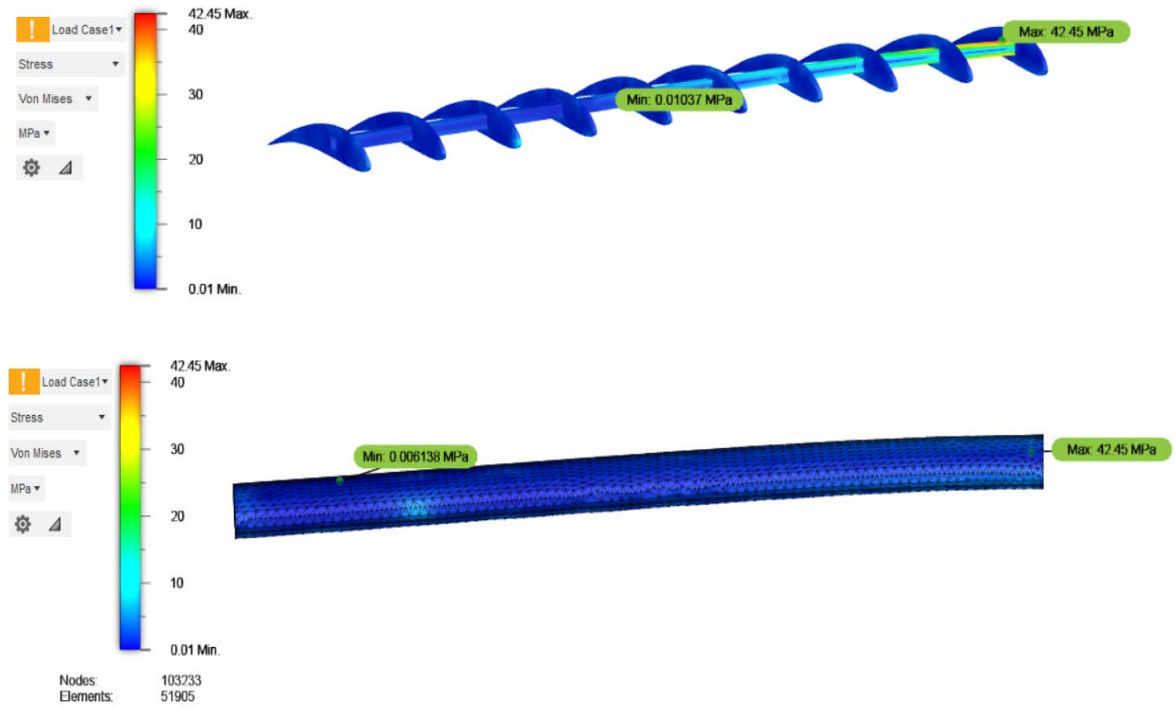


Fig. 7.15. Point of maximum and minimum stress

### 7.3.5. INFERENCE

The maximum displacement obtained from the static stress analysis = 9.267 mm

Maximum Von Mises stress value = 42.45 MPa

Minimum Von Mises stress value = 0.01037 MPa

The obtained values for displacement and stress are within the safe limits and hence the chosen materials are safe to use.

# CHAPTER 8

# MATERIAL SELECTION & COST ANALYSIS

## 8.1. MATERIALS SELECTED FOR HYBRID UAV

This section describes the materials selected for the manufacture of the aircraft. For selection of materials, appropriate market study was conducted. Detailed discussion of the electronic components has been given in Chapter 5. The materials selected for the covering and structure of aircraft has been given here.

### 8.1.1. BIRCH WOOD

Birch wood is a common material which is used in RC aircrafts. The reason for selecting birch wood is that it has got a high strength-to-weight ratio. It has properties such as high strength, low density and can be shaped, sanded, glued and painted according to the requirement.

In this project, 5mm birch wood sheets were selected to make the wing ribs. The birch wood sheet is cut in the shape of the wing rib (both main wing and tail) and they are glued on to the wing spar. The main purpose of adding ribs is to provide the required shape to the wing and to add strength to the wing. The properties of the birch wood are as follows:

i. High impact strength
ii. High strength-to-weight ratio
iii. Flexible
iv. Light weight

Fig. 8.1. Birch Wood Sheets

### 8.1.2. ALUMINIUM SQUARE SECTION ROD

Aluminium is one of the most commonly preferred and used material for adding structural strength to aircrafts including RC aircrafts.

The wing structure contains a single aluminium spar, extending from the wing root to tip through the birch wood ribs. The selected aluminium section has a dimension of 12.7 x 12.7 mm. The alloy selected here was Al 7075.

The desirable properties that led to Al 7075 being selected as the central stem of the aircraft and for holding the wing cross sections are:

i. **High strength-to-weight ratio** - Aluminium has a very high strength-to-weight ratio. This allows to maintain the overall weight of the aircraft at a minimum when compared to other materials like steel.

ii. **High corrosion resistance** - Aluminium is resistant to corrosion. This allows the aircraft to have a longer life and retain its structural strength over a longer time.

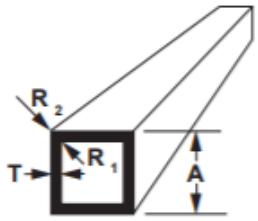


| A | T | $R_1$ | $R_2$ | Kg/m |
|---|---|---|---|---|
| 12.70 | 1.65 | | | 0.197 |

Fig. 8.2. Aluminium rod

### 8.1.3. MONOKOTE

MonoKote is a lightweight plastic shrink wrap used to cover the surfaces of model aircrafts. It is available in opaque, flat, transparent, metallic, pearl and neon finishes. It is sold in a sheet form that is cut to size and applied to the aircraft surfaces. The adhesive backing of the MonoKote is activated using a heating iron. The MonoKote is used for the skin of the wing and fuselage.

### 8.1.4. ABS

Although there are dozens of materials available for 3D printing, the two most popular materials used are polylactic acid (PLA) and acrylonitrile butadiene styrene (ABS). ABS is more popular because of its low cost and easy availability. For printing, ABS needs a temperature ranging from 215° to 250°C (420° to 480°F). Despite the higher temperature, ABS is easier to extrude, requiring less force. Its extrusion characteristics make it better for printing small, detailed parts.

ABS is used in this project to model the nose of the aircraft. The battery-&-flight-control holder (shown in Fig. 7.8.) is also to be 3D printed with ABS.

## 8.2. WEIGHT BUILD UP CHART

Table 8.1. Weight Build-up of components

| **Parts** | **Weight (g wt.)** |
|---|---|
| Horizontal Motor | 221 |
| Propeller (FW) | 130 |
| ESCs (FW) | 82 |
| Quadrotor Motors (4 no.s) | 996 |
| ESCs -Quad (4 no.s) | 252 |
| Propellers-Quad (4 no.s) | 240 |
| Battery | 1400 |
| Aluminium section (3 m) | 600 |
| Nose (ABS) | 300 |
| Battery Holder (ABS) | 250 |
| Wing Cross Sections (Birch) | 250 |
| Fuselage cross section (Birch) | 400 |
| Skin | 50 |
| Wiring | 70 |
| Bolts and Nuts | 100 |
| **Total** | 5341 |

## 8.3. COST ANALYSIS

This section shows the cost that would be incurred in the manufacture of the hybrid UAV.

Table 8.2. Cost Analysis Chart

| **Parts** | **Cost (₹ )** |
|---|---|
| Horizontal Motor | 6000 |
| Propeller (FW) | 4500 |
| ESCs (FW) | 2700 |
| Quadrotor Motors (4 no.s) | 24000 |
| ESCs -Quad (4 no.s) | 10800 |
| Propellers-Quad (4 no.s) | 16000 |
| Battery | 7000 |
| Aluminium section (3 m) | 1000 |
| Birch Wood Sheets | 3000 |
| MonoKote | 1500 |
| Joining Materials | 1000 |
| Manufacturing | 5000 |
| Miscellaneous | 3000 |
| **Total** | **₹ 85500** |

# CHAPTER 9

# FLIGHT CONTROL SYSTEM

The complexity of the dynamics of aerial vehicles makes obtaining accurate mathematical models for a large portion of flight envelope, a difficult problem. Hence, an approximate approach involving resolving the various force vectors involved in the flight dynamics, and computing their resultants is adopted here.

The hybrid UAV was modelled as two independent aerial platforms, where quadrotor dynamics and fixed wing dynamics were separately modelled. When only one mode is in operation, this is certainly a true assumption. However, during flight mode transition, both flight motors are in operation, which causes coupling between the two dynamic models. These coupling effects between the two models can be considered to be short lasting disturbances that are to be rejected by the feedback controls in each flight mode controller. Flight dynamics of both modes were modelled in MATLAB Simulink, and through simulation results, important model coefficients were determined. The approach followed is detailed in this chapter.

## 9.1. EMPIRICAL MODELLING OF QUADROTOR MOTORS

The response of the motors to applied voltage has to be determined for application in the MATLAB model. Here, this response was determined using the motor data available from the spec sheet in the motor manufacturer's website.

Here, the motor selected is **T-Motor MN5212 KV340** with **17" * 5.8"** propellers.

### 9.1.1. VOLTAGE VS RPM RESPONSE

From the spec sheet, it is seen that there is a percentage drop of 18% in the loaded RPM from the unloaded RPM response. Taking this into consideration, the data from the spec sheet was tabulated and plotted in Excel and the relation between voltage and loaded RPM was determined.

Table 9.1. RPM response of quadrotor motor

| Voltage | Percentage Drop in RPM (actual) | No Load RPM | Loaded RPM |
|---|---|---|---|
| 0 | 0 | 0 | 0 |
| 1.2 | 0.009 | 408 | 404.328 |
| 2.4 | 0.018 | 816 | 801.312 |
| 3.6 | 0.027 | 1224 | 1190.952 |
| 4.8 | 0.036 | 1632 | 1573.248 |
| 6 | 0.045 | 2040 | 1948.2 |
| 7.2 | 0.054 | 2448 | 2315.808 |
| 8.4 | 0.063 | 2856 | 2676.072 |
| 9.6 | 0.072 | 3264 | 3028.992 |
| 10.8 | 0.081 | 3672 | 3374.568 |
| 12 | 0.09 | 4080 | 3712.8 |
| 13.2 | 0.099 | 4488 | 4043.688 |
| 14.4 | 0.108 | 4896 | 4367.232 |
| 15.6 | 0.117 | 5304 | 4683.432 |
| 16.8 | 0.126 | 5712 | 4992.288 |
| 18 | 0.135 | 6120 | 5293.8 |
| 19.2 | 0.144 | 6528 | 5587.968 |
| 20.4 | 0.153 | 6936 | 5874.792 |
| 21.6 | 0.162 | 7344 | 6154.272 |
| 22.8 | 0.171 | 7752 | 6426.408 |
| 24 | 0.18 | 8160 | 6691.2 |

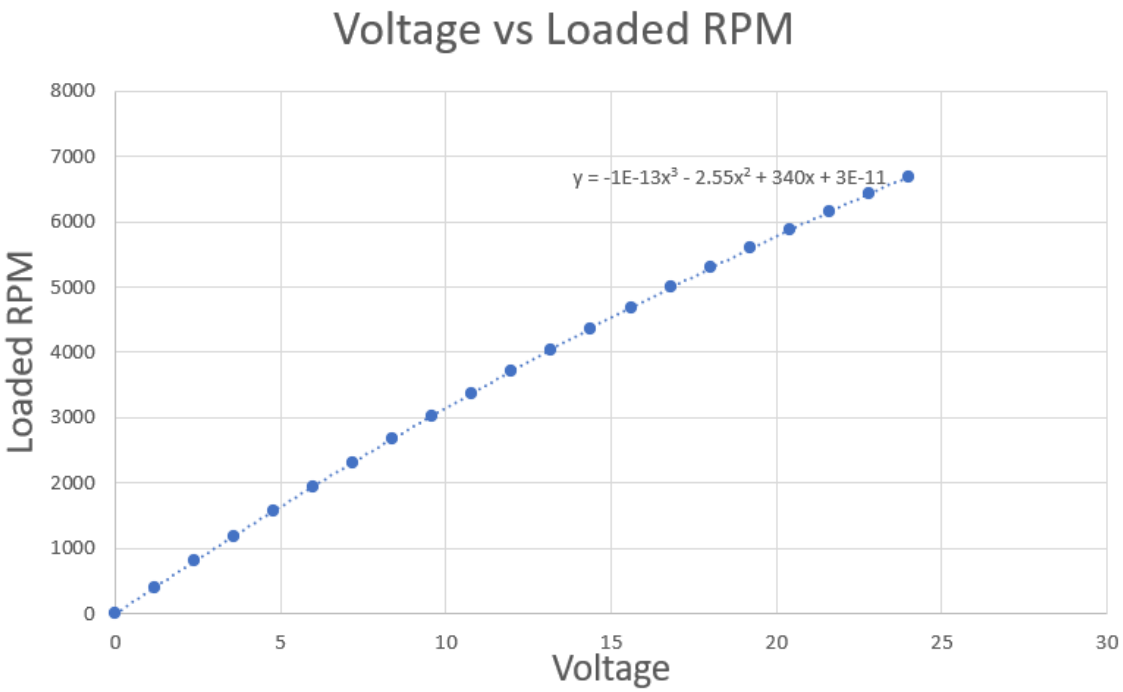


Fig. 9.1. Voltage vs RPM plot of quadrotor motor

The relation was found to be

$$RPM = (-1 \times 10^{-13})V^3 - 2.55V^2 + 340V + (3 \times 10^{-11}) \quad (9.1)$$

### 9.1.2. RPM VS THRUST RESPONSE

From the spec sheet, the RPM and thrust response for applied throttle was taken, and the response relation was found.

Table 9.2. Thrust response of quadrotor motor

| Throttle (%) | RPM | Thrust (g) |
|---|---|---|
| 0 | 0 | 0 |
| 50 | 3651 | 1095 |
| 55 | 4017 | 1320 |
| 60 | 4432 | 1625 |
| 65 | 4772 | 1875 |
| 75 | 5390 | 2363 |
| 85 | 5960 | 2871 |
| 100 | 6660 | 3716 |

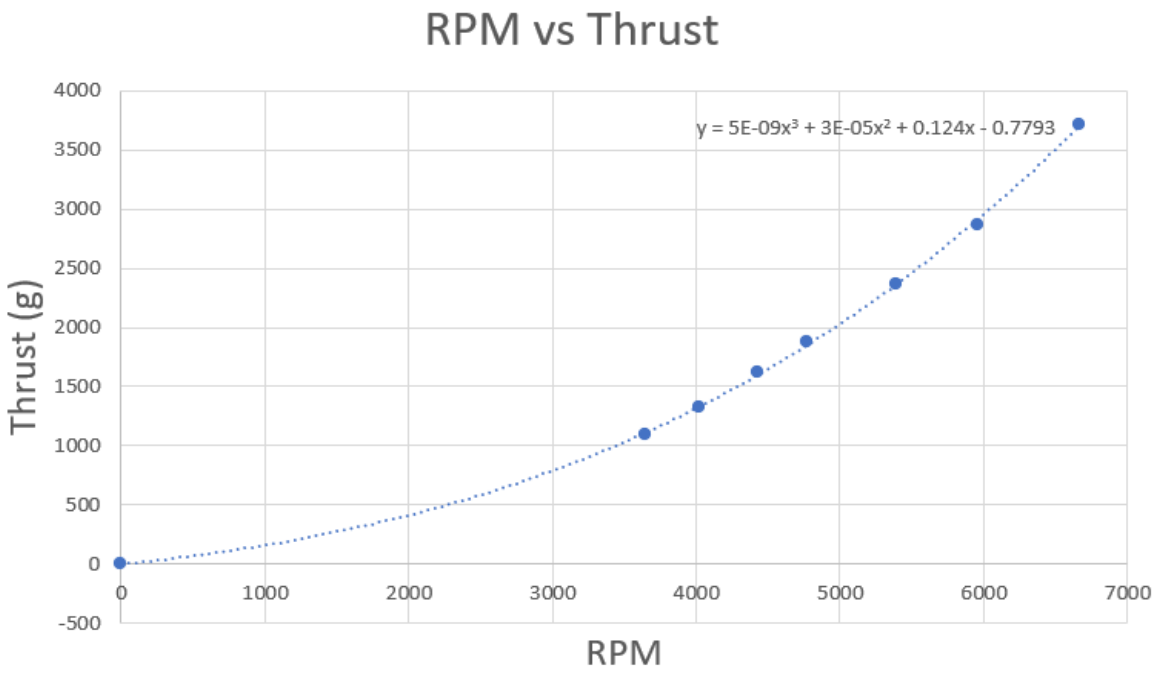


Fig. 9.2. RPM vs Thrust plot of quadrotor motor

The RPM-thrust relation was found to be

$$Thrust \quad F = (5 \times 10^{-9})RPM^3 + (3 \times 10^{-5})RPM^2 + 0.124RPM - 0.7793 \tag{9.2}$$

### 9.1.3. RPM VS TORQUE RESPONSE

From the spec sheet, the RPM and thrust response for applied throttle was taken, and the response relation was found.

Table 9.3. Torque response of quadrotor motor

| Throttle (%) | RPM | Torque (N.m) |
|---|---|---|
| 0 | 0 | 0 |
| 50 | 3651 | 0.225 |
| 55 | 4017 | 0.27 |
| 60 | 4432 | 0.331 |
| 65 | 4772 | 0.381 |
| 75 | 5390 | 0.49 |
| 85 | 5960 | 0.593 |
| 100 | 6660 | 0.761 |

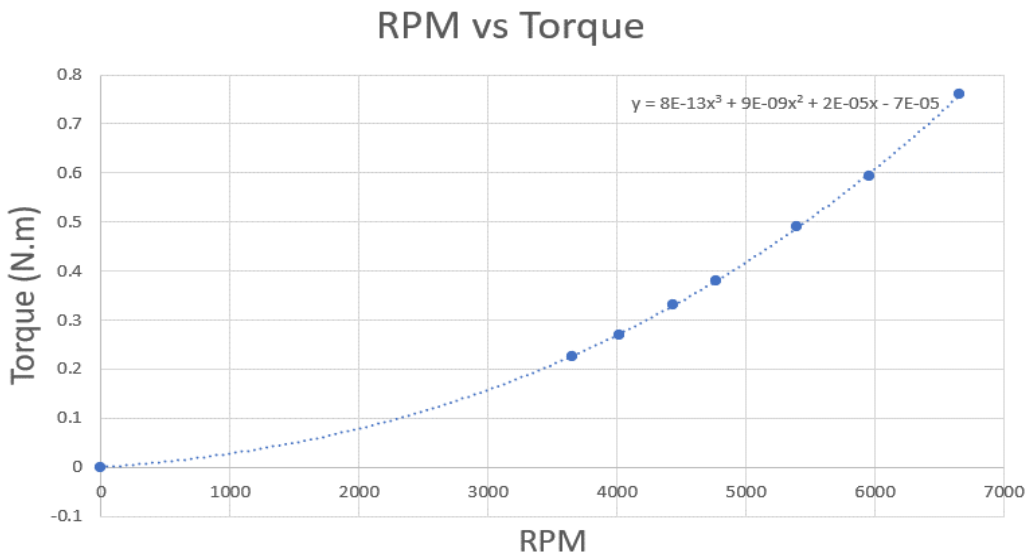


Fig 9.3. RPM vs Torque plot of quadrotor motor

The RPM-thrust relation was found to be

$$Torque \quad T = (8 \times 10^{-13})RPM^3 + (9 \times 10^{-9})RPM^2 + (2 \times 10^{-5})RPM - (7 \times 10^{-5}) \tag{9.3}$$

## 9.2. EMPIRICAL MODELLING OF HORIZONTAL MOTORS

The response of the horizontal motor to applied voltage also has to be determined for application in the MATLAB model. Here too, this response was determined using the motor data available from the spec sheet in the motor manufacturer's website.

Here, the motor selected was **T-Motor AT3520 Long Shaft KV850** with **APC 14" * 7"** propellers.

### 9.2.1. VOLTAGE VS RPM RESPONSE

From the spec sheet, it is seen that there is a percentage drop of 31.65% in the loaded RPM from the unloaded RPM response. Taking this into consideration, the data from the spec sheet was tabulated and plotted in Excel and the relation between voltage and loaded RPM is determined.

Table 9.4. RPM response of horizontal motor

| Voltage (V) | Percentage Drop in RPM (actual) | No Load RPM | Loaded RPM |
|---|---|---|---|
| 0 | 0 | 0 | 0 |
| 0.74 | 0.015825 | 629 | 619.046075 |
| 1.48 | 0.03165 | 1258 | 1218.1843 |
| 2.22 | 0.047475 | 1887 | 1797.414675 |
| 2.96 | 0.0633 | 2516 | 2356.7372 |
| 3.7 | 0.079125 | 3145 | 2896.151875 |
| 4.44 | 0.09495 | 3774 | 3415.6587 |
| 5.18 | 0.110775 | 4403 | 3915.257675 |
| 5.92 | 0.1266 | 5032 | 4394.9488 |
| 6.66 | 0.142425 | 5661 | 4854.732075 |
| 7.4 | 0.15825 | 6290 | 5294.6075 |
| 8.14 | 0.174075 | 6919 | 5714.575075 |
| 8.88 | 0.1899 | 7548 | 6114.6348 |
| 9.62 | 0.205725 | 8177 | 6494.786675 |
| 10.36 | 0.22155 | 8806 | 6855.0307 |
| 11.1 | 0.237375 | 9435 | 7195.366875 |
| 11.84 | 0.2532 | 10064 | 7515.7952 |
| 12.58 | 0.269025 | 10693 | 7816.315675 |
| 13.32 | 0.28485 | 11322 | 8096.9283 |
| 14.06 | 0.300675 | 11951 | 8357.633075 |
| 14.8 | 0.3165 | 12580 | 8598.43 |

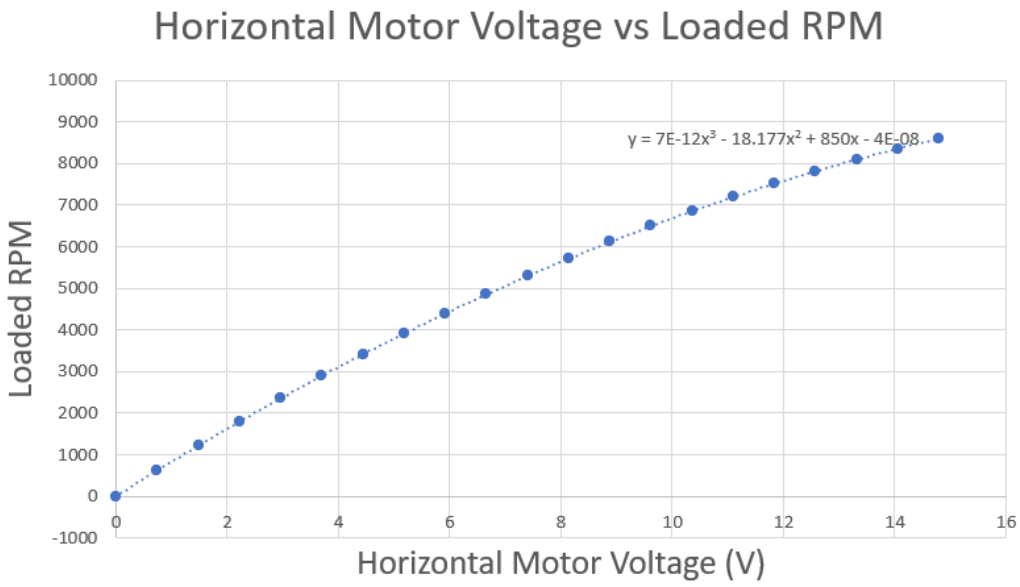


Fig 9.4. Voltage vs RPM plot of horizontal motor

The relation was found to be

$$RPM = (7 \times 10^{-12})V^3 - 18.177V^2 + 850V - (4 \times 10^{-8}) \quad (9.4)$$

### 9.2.2. RPM VS THRUST RESPONSE

From the spec sheet, the RPM and thrust response for applied throttle was taken, and the response relation was found.

Table 9.5. Thrust response of horizontal motor

| Throttle (%) | RPM | Thrust (g) |
|---|---|---|
| 0 | 0 | 0 |
| 40 | 4578 | 1021 |
| 45 | 4937 | 1214 |
| 50 | 5432 | 1468 |
| 55 | 5928 | 1785 |
| 60 | 6323 | 2033 |
| 65 | 6746 | 2323 |
| 70 | 7071 | 2570 |
| 75 | 7435 | 2852 |
| 80 | 7743 | 3111 |
| 90 | 8318 | 3607 |
| 100 | 8598 | 3854 |

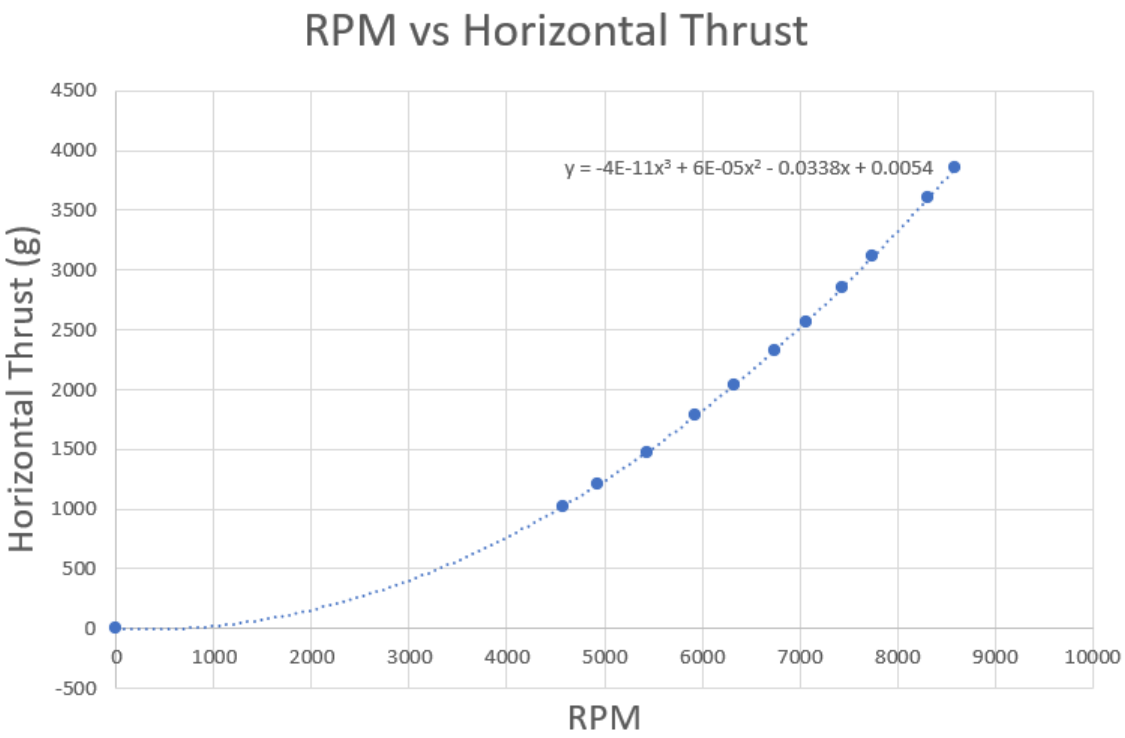


Fig 9.5. RPM vs Horizontal Thrust plot

The RPM-horizontal thrust relation was found to be

$$Thrust \quad HF = (-4 \times 10^{-11})RPM^3 + (6 \times 10^{-5})RPM^2 - 0.0338RPM + 0.0054 \tag{9.5}$$

## 9.3. MOTOR MIXING ALGORITHM

The individual thrust, roll, pitch and yaw inputs is given in terms of percentages of throttle. These inputs have to be split into individual signals to each individual motor. This is done using the motor mixing algorithm.

Motor mixing algorithm is given by

$$V_1 = Throttle - Pitch - Roll - Yaw \tag{9.6}$$

$$V_2 = Throttle - Pitch + Roll + Yaw \tag{9.7}$$

$$V_3 = Throttle + Pitch + Roll - Yaw \tag{9.8}$$

$$V_4 = Throttle + Pitch - Roll + Yaw \tag{9.9}$$

where $V_1$, $V_2$, $V_3$ and $V_4$ are the voltages that should be input to motors 1, 2, 3 and 4.

The code for the motor mixing algorithm is given in Appendix 2.1.

## 9.4. ROTATIONAL DYNAMICS

In this section, we describe and model the rotational effects that act on the drone, due to the various forces and torques produced by the propellers.

### 9.4.1. YAW MOTION

Yaw motion is the rotation of the drone about the z-axis. Therefore, for implementing yaw motion, the rotational moment about the z-axis, $M_z$ is varied.

Taking clockwise rotation around z-axis, when observed from the top, to be positive, the resultant moment about z-axis is

$$M_z = T_4 - T_1 + T_2 - T_3 \tag{9.10}$$

where $T_1$, $T_2$, $T_3$ and $T_4$ are the torques generated by the propellers 1, 2, 3 and 4.

Angular acceleration in z-direction,

$$\alpha_z = \frac{M_z}{I_z} \tag{9.11}$$

For rotating the drone in the clockwise direction, the speed of propellers 1 and 3 are increased, and that of propellers 2 and 4 are correspondingly decreased. This would result in a net rotational moment in the counter clockwise direction. According to Newton's Third Law of Motion, the drone will tend to have a clockwise moment to balance this moment induced due to the variation in the propeller speeds, and thus rotate in the clockwise direction.

Similarly, for rotating the drone in the counter clockwise direction, the speed of propellers 2 and 4 are increased, and that of propellers 1 and 3 are correspondingly decreased. This results in a rotational moment in the counter clockwise direction to balance the moment induced due to the variation in the propeller speeds, and thus, the drone will rotate in the counter clockwise direction.

Here, we consider clockwise rotation as positive yaw and counter clockwise rotation as negative yaw, as when observed from the top.

### 9.4.2. PITCH MOTION

Pitch motion is the rotation of the drone about the x-axis. Therefore, for implementing pitch motion, the rotational moment about the x-axis, $M_x$ is varied.

Here, we consider pitching forward as positive pitch, and pitching backwards as negative pitch. The resultant moment about the x-axis is given by

$$M_x = (F_3 + F_4) \times 0.301 - (F_1 + F_2) \times 0.301 \quad (9.12)$$

where $F_1$, $F_2$, $F_3$ and $F_4$ are the forces generated by the propellers 1,2,3 and 4.

Angular acceleration in x-direction,

$$\alpha_x = \frac{M_x}{I_x} \quad (9.13)$$

For pitching positively or pitching forward, the speeds of propellers 3 and 4 are increased and that of propellers 1 and 2 are correspondingly decreased, creating a positive pitching moment. Similarly, for pitching negatively or pitching backwards, the speeds of propellers 1 and 2 are increased and that of propellers 3 and 4 are correspondingly decreased, creating a negative pitching moment.

### 9.4.3. ROLL MOTION

Roll motion is the rotation of the drone about the y-axis. Therefore, for implementing roll motion, the rotational moment about the y-axis, $M_y$ is varied.

Here, we consider rolling clockwise as positive roll, and rolling counter clockwise as negative roll. The resultant moment about the y-axis is given by

$$M_y = (F_2 + F_3) \times 0.5635 - (F_1 + F_4) \times 0.5635 \quad (9.14)$$

where $F_1$, $F_2$, $F_3$ and $F_4$ are the forces generated by the propellers 1,2,3 and 4.

Angular acceleration in y-direction,

$$\alpha_y = \frac{M_y}{I_y} \quad (9.15)$$

For rolling positively or rolling clockwise, the speeds of propellers 2 and 3 are increased and that of propellers 1 and 4 are correspondingly decreased, creating a positive rolling moment. Similarly, for rolling negatively or rolling counter clockwise, the speeds of propellers 1 and 4 are increased and that of propellers 2 and 3 are correspondingly decreased, creating a negative rolling moment.

The equations described in the above section are coded as MATLAB functions, as shown in Appendix 2.3.

## 9.5. LINEAR DYNAMICS

In this section, we describe and model the various linear effects that come into play during the operation of the drone, due to the forces produced by the propellers and the real-time attitude of the drone.

### 9.5.1. ROLL AND PITCH THRUST VECTORS

Let us consider that the drone is operation, and has a positive pitch angle $\theta_x$ and a positive roll angle $\theta_y$.

Then, the force produced by the propellers in the x-direction will be given by

$$F_{prop_x} = (F_1 + F_2 + F_3 + F_4) \times \sin\theta_y \times \cos\theta_x \quad (9.16)$$

that in the y-direction will be given by

$$F_{prop_y} = (F_1 + F_2 + F_3 + F_4) \times \sin\theta_x \times \cos\theta_y \quad (9.17)$$

and that in the z-direction will be given by

$$F_{prop_z} = (F_1 + F_2 + F_3 + F_4) \times \cos\theta_x \times \cos\theta_y \quad (9.18)$$

### 9.5.2. YAW THRUST VECTOR

When the drone also has a yaw input, calculation of the resultant thrust becomes more complex.

The resultant of the forces in the XY plane is given by

$$XY_{2D} = \sqrt{{F_{prop_x}}^2 + {F_{prop_y}}^2} \quad (9.19)$$

and its angle with the y-axis is given by

$$\theta_{XY} = -\tan\left(\frac{F_{prop_x}}{F_{prop_y}}\right) \quad (9.20)$$

Then, we can rewrite $F_{prop_x}$ and $F_{prop_y}$ as

$$F_{prop_x} = XY_{2D} \times \sin(\theta_{XY} \pm \theta_z) \quad (9.21)$$

$$F_{prop_y} = XY_{2D} \times \cos(\theta_{XY} \pm \theta_z) \quad (9.22)$$

The equations described in the above section are coded as MATLAB functions, as shown in Appendix 2.4.

### 9.5.3. SUM OF LINEAR FORCES

We can now calculate the net force in the x, y, and z directions.

Force in x-direction, $$F_x = F_{prop_x} \pm Drag_x \quad (9.23)$$

Force in y-direction, $$F_y = HF + F_{prop_y} \pm Drag_y \quad (9.24)$$

where 'HF' is the horizontal thrust produced by the horizontal motor.

Force in z-direction, $$F_z = F_{prop_z} - mg \pm Drag_z \quad (9.25)$$

where 'm' is the mass of the aircraft in kg and 'g' is the acceleration due to gravity in m/s$^2$.

Drag in the x-direction, $$Drag_x = \frac{1}{2}\rho {V_x}^2 A_x C_d \quad (9.26)$$

Drag in the y-direction, $$Drag_y = \frac{1}{2}\rho {V_y}^2 A_y C_d \quad (9.27)$$

Drag in the z-direction, $$Drag_z = \frac{1}{2}\rho {V_z}^2 A_z C_d \quad (9.28)$$

From the resultant forces, the acceleration of the drone in each direction is determined.

Acceleration in the x-direction,

$$a_x = \frac{F_x}{m} \quad (9.29)$$

Acceleration in the y-direction,

$$a_y = \frac{F_y}{m} \quad (9.30)$$

Acceleration in the z-direction,

$$a_z = \frac{F_z}{m} \quad (9.31)$$

## 9.6. FEEDBACK LOOPS

The output of the rotational dynamics block is the angular acceleration of the drone in the x, y and z directions. On integrating this output, we obtained the angular velocity, and on further integrating, we obtained the angular position of the drone.

Similarly, the output of the linear dynamics block is the linear acceleration of the drone in the x, y and z directions. On integrating this signal, we obtained the linear velocity, and on further integrating, we obtained the linear position of the drone.

Then, a closed loop control system was implemented to stabilise the system, compensate for disturbances, reduce sensitivity to parameter variation and to make it implementable for real world applications. It was also used to implement automated flight to the desired destination.

Proportional-integral-derivative (PID) controllers were used here, due to their ease of applicability in real world situations. PID controllers also rely on data available from sensors and doesn't rely on the underlying process that often contains unknowns, uncertainties and disturbances. A major drawback of this controller is that it does not guarantee optimal control or closed-loop system stability, and hence requires fine tuning for satisfactory performance.

We have implemented five feedback loops in this control system, each controlling a specific flight parameter. The parameters being controlled are horizontal thrust, altitude, pitch, roll, and yaw.

The PID controllers have to be tuned to attain stability. Tuning PID controllers is the process of adjusting the control parameters [$k_p$ $k_i$ $k_d$] to optimum values for the desired control purpose. Here, $k_p$ is called the proportional gain, $k_i$ is called the integral gain and $k_d$ is called the derivative gain. The performance of the closed-loop system depends on the transient, as well as the steady-state behaviour, and is usually specified in terms of rise time, settling time, percentage overshoot and steady state error.

## 9.7. RESULT OF SIMULATION

The quadplane simulation was done using the closed-loop control system for a simulation time of 60 seconds. The altitude reference for the altitude controller was set at 50m and the destination was set as (100,100). The pitch and roll stabilizer PID controllers are used to stabilize the drone in case of external factors such as wind gusts. The roll and pitch angle references for these controllers was set at $0^{\circ}$. The yaw angle was calculated using a MATLAB function (Appendix 2.5.) and then used as the reference for the yaw controller. The horizontal thrust was controlled using the thrust controller, which used the destination coordinates as the reference.

The PID controllers were then tuned for stability and optimum steady state response.

Despite multiple iterations of manual tuning of all the PID controllers, we were unable to attain a steady state response for the position of the drone. However, we obtained a steady state response with zero steady state error for the altitude controller.

The most optimum values found for the PID controller gains are:

1. Thrust Controller

   **[$k_p$ = 0.0001 $k_i$ = 400 $k_d$ = 50] N = 15**

2. Altitude Controller

   **[$k_p$ = 15 $k_i$ = 140.1 $k_d$ = 20] N = 100**

3. Pitch Stabilizer

   **[$k_p$ = 100 $k_i$ = 5 $k_d$ = 5] N = 10**

4. Roll Stabilizer

   **[$k_p$ = 100 $k_i$ = 5 $k_d$ = 5] N = 14.222**

5. Yaw Controller

   **[$k_p$ = 1563.202 $k_i$ = 0.041178 $k_d$ = 550] N = 100**

where 'N' is the filter coefficient.

The response plots obtained for the above simulation are shown below -

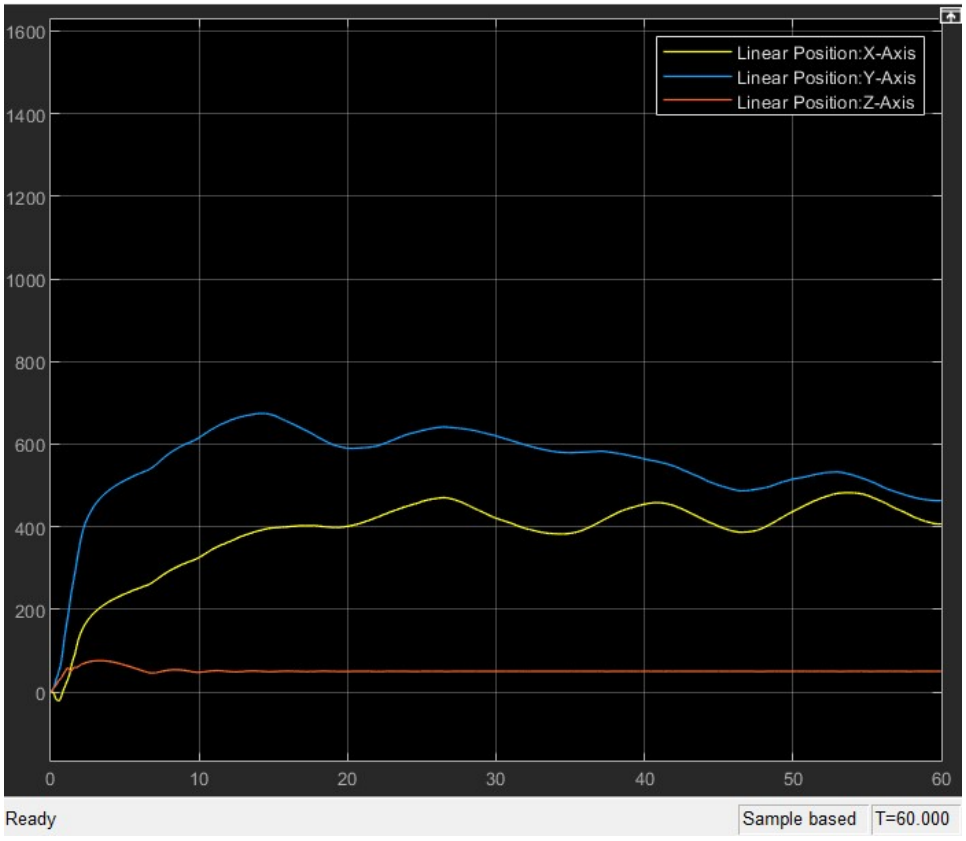


Fig 9.6. Linear Position

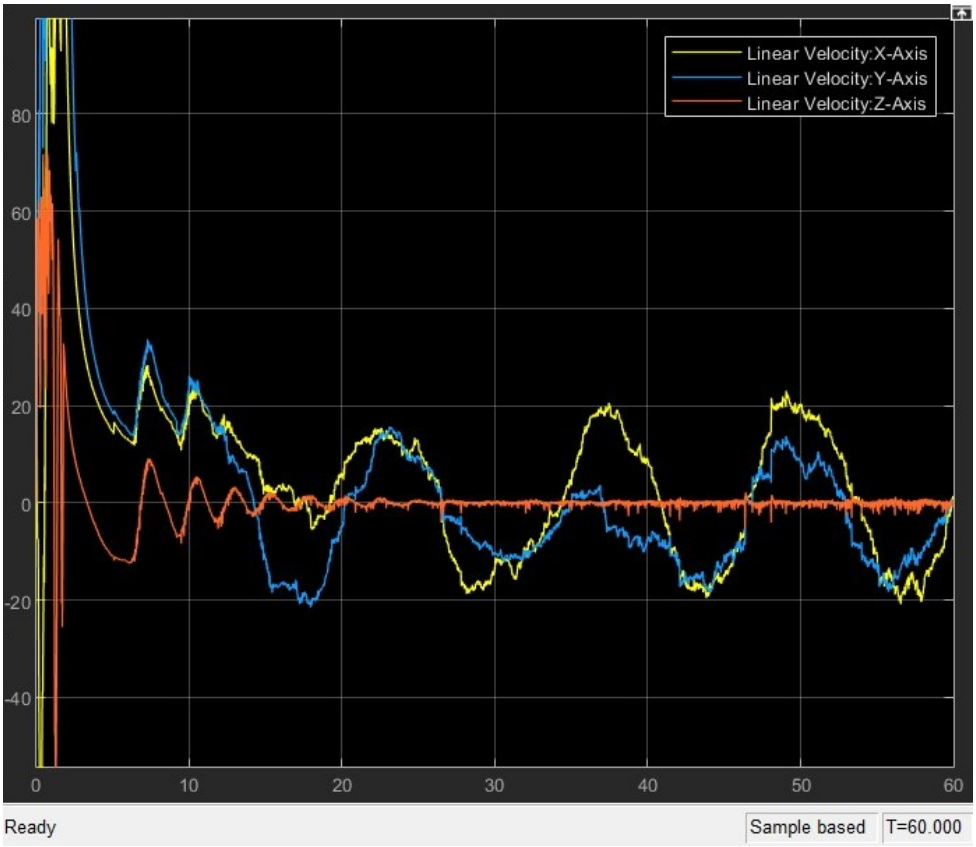


Fig 9.7. Linear Velocity

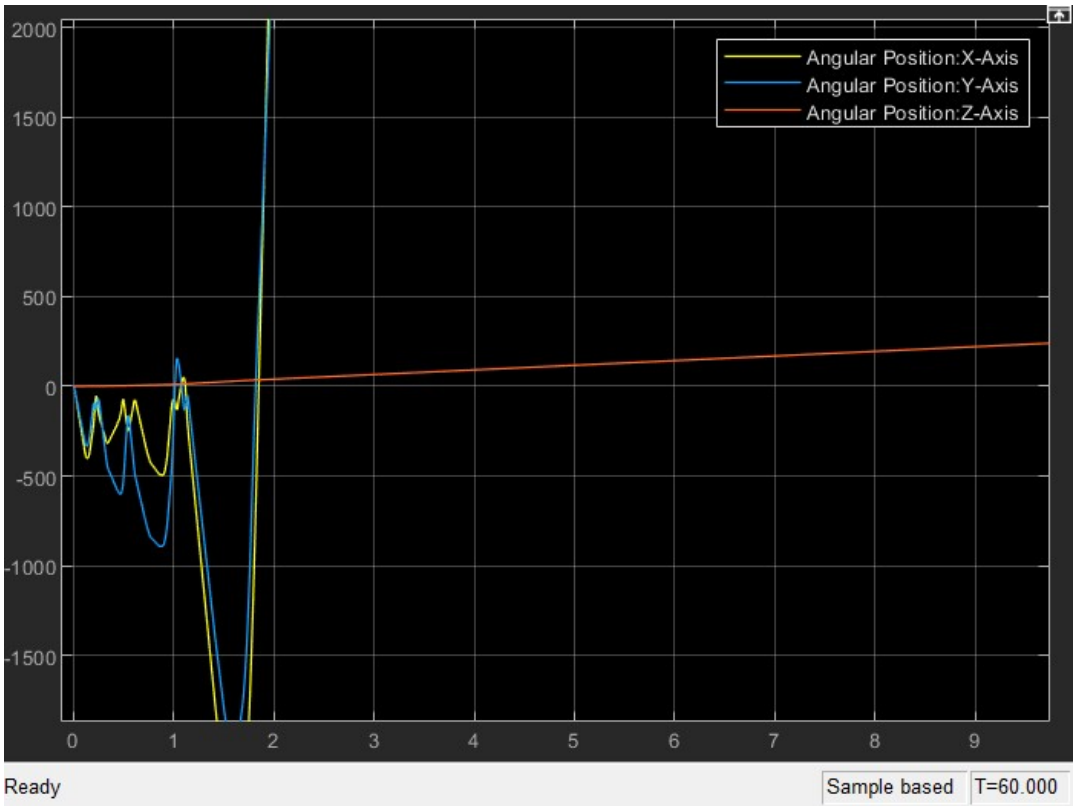


Fig 9.8. Angular Position

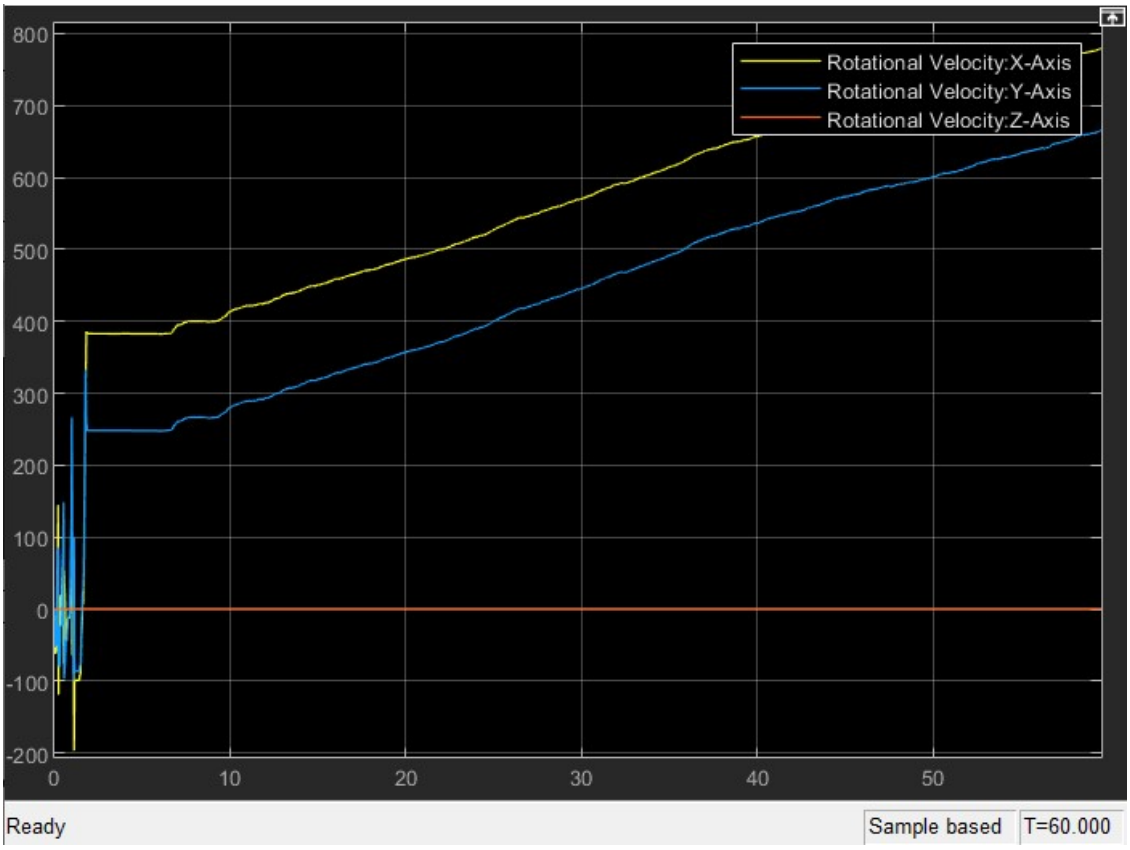


Fig 9.9. Angular Velocity

These results were most likely due to the specific approach followed here for constructing the flight control system. This particular approach was adopted due to it being less complex and easy to model, as well as to complete the project within the stipulated time.

Therefore, to obtain better results, we will have to reconstruct the flight control system in a better way, i.e. by developing a linearised form of the state-space model of the quadplane.

The code for the various MATLAB functions used to create the Simulink model is given in Appendix 2.

The Simulink model created is shown in Appendix 3.

# CHAPTER 10

# CONCLUSION

This project mainly emphasises on the design of mechanical, electronics and control part of a quadplane. We were able to design and size the UAV with the required parameters, which would be optimum for the medical transportation purpose.

First, we began with fixing the wing planform dimensions. Fixing an appropriate aircraft cruising velocity, various parameters such as Reynolds number, design coefficient of lift, stall velocity, thrust required, etc. were determined. Using the design lift coefficient, a suitable airfoil with the required angle of attack was selected.

In the next step, various parameters that affect the stability of the aircraft such as position of neutral point, centre of gravity, aerodynamic centre, sizing and lever arm lengths of vertical and horizontal stabilizers, etc. were calculated.

Then, the structural analysis of the wing was performed, ensuring its safety. We had also intended to perform a CFD analysis of the quadplane. However, due to the continued spread of the pandemic and lack of adequate computational facilities, we were unable to do the same. The pre-planned fabrication of the quadplane was also put on hold due to the pandemic restrictions.

The aforementioned limitations led us to develop and simulate a flight control system in MATLAB. The properties of the motors used were modelled in Simulink, using data from the manufacturer spec sheet. Properties of the quadplane such as moment of inertia, planform area, etc. were also integrated into the Simulink model. Then, the rotational and linear dynamics of the quadplane was modelled. Closed loops with PID controllers were also created to implement automated flight of the quadplane to a given positional coordinate. However, due to problems in the approach adopted, we were not able to make the position response of the quadplane reach steady state. Tuning the gain values of the PID controllers did not help achieve zero steady state error.

In the future, we need to build a more complex control system which could then be properly tuned to achieve steady state response during operation. The study reported in this project can form a base for further research to develop a practical, hybrid UAV with high working efficiency and safety measures.

# REFERENCES


[1] B. Defense, “V-22 osprey,” Space and Security.

[2] D. C. Dugan, “Thrust control of vtol aircraft part deux,” in the 5th Decennial Aeromechanics Specialists Conf, January 2014.

[3] B. Handy, “Harrier gr7,” Royal Air Force Aircraft and Weapons, pp. 8–9.

[4] S. Carlson, “A hybrid tricopter/flying-wing vtol uav.” American Institute of Aeronautics and Astronautics

[5] D. D. Sander Hulsman, Jurjen de Groot, “Atmos uav,” Leonardo Times, March 2013.

[6] S. J. Yong, J. Y. You and O. J. Kwon, “Numerical investigation of prop-rotor and tail-wing aerodynamic interference for a tilt-rotor UAV configuration”, Journal of Mechanical Science and Technology. J., vol. 28, no. 7, pp. 2609–2617, July 2014.

[7] G. Cai, B. M. Chen, and T. H. Lee, Unmanned rotorcraft systems. Springer Science & Business Media, 2011.

[8] K. T. Oner, E. C¸ etinsoy, E. Sırımo ¨ glu, C. Hancer, T. Ayken, and ˘ M. Unel, “Lqr and smc stabilization of a new unmanned aerial ¨ vehicle,” 2009

[9] Alaukik Joshi, Amritanshu Tripathi, Ponnalgu R. N, “Modelling and Design of a Hybrid Aerial Vehicle Combining VTOL Capabilities with Fixed Wing Aircraft”, International Conference on Instrumentation, Control, and Automation (ICA) Bandung, Indonesia. 31 July – 2 August 2019

[10] M. Nagai, T. Chen, R. Shibasaki, H. Kumagai and A. Ahmed, "UAVborne 3-d mapping system by multisensor integration," in Geoscience and Remote Sensing, IEEE Transactions, 2009, pp. 701-708.

[11] V. Ramanathan, M. Ramana, G. Roberts, D. Kim, C. Corrigan, C. Chung and D. Winker, "Warming trends in asia amplified by brown cloud solar absorption," in Nature, 2007, pp. 575-578.

[12] A. R. Girard, A. S. Howell and J. K. Hedrick, "Border patrol and surveillance missions using multiple unmanned air vehicles," in Decision and Control, 2004. CDC. 43rd IEEE Conference, 2004, pp. 620-625

[13] G. Grenzdorffer, A. Engel and B. Teichert, "The photogrammetric potential of low-cost uavs in forestry and agriculture," in International Archives of the Photogrammetry, Remote Sensing and Spatial Information Sciences, 2008, pp. 1207-1214

[14] S. Herwitz, L. Johnson, S. Dunagan, R. Higgins, D. Sullivan, J. Zheng, B. Lobitz, J. Leung, B. Gallmeyer and M. Aoyagi, "Imaging from an unmanned aerial vehicle: agricultural surveillance and decision support," in Computers and electronics in agriculture, 2004, pp. 49-61.

[15] S. Waharte and N. Trigoni, "Supporting search and rescue operations with UAVs," in Emerging Security Technologies (EST), IEEE, 2010, pp. 142-147.

[16] L. Geng, Y. Zhang, J. Wang, J. Fuh and S. Teo, "Mission planning of autonomous uavs for urban surveillance with evolutionary algorithms," in Control and Automation (ICCA), IEEE, 2013, pp. 828-833.

[17] N. H. Motlagh, M. Bagaa and T. Taleb, "UAV-Based IoT Platform: A Crowd Surveillance Use Case," in IEEE Communications Magazine, Sejong, 2017, pp. 128 - 134.

[18] W. Liu, G. He, H. Yu, T. Li and J. Zhang, "Review on dynamic modeling of tilt-rotor UAVs in low-speed flight," in International Conference on Sensing, Diagnostics, Prognostics and Control, IEEE, 2018, pp. 284-290.

[19] W. Lu, D. Zhang, J. Zhang, T. Li and T. Hu, "Design and Implementation of a Gasoline-Electric Hybrid Propulsion System for a Micro Triple Tilt-rotor VTOL UAV," in IEEE 6th Data Driven Control and Learning Systems Conference, Chongqing, 2017.

[20] G. Ducard and M. Hua, "Modeling of an Unmanned Hybrid Aerial Vehicle," in Conference on Control Applications (CCA), IEEE, Antibes, 2014, pp. 1011-1016.

[21] Kitonsa, H., Kruglikov, S.V., 2018. Significance of drone technology for achievement of the United Nations sustainable development goals. R-Economy 4, 115–120.

[22] McKinsey, 2016b. Parcel Delivery: The Future of Last Mile.

[23] Horváth & Partners, 2019. Urban Air Mobility Study Report 2019. Stuttgart.

[24] Alwateer, M., Loke, S.W., Zuchowicz, A.M., 2019. Drone services: issues in drones for location-based services from human-drone interaction to information processing. Journal of Location Based Services, 1–34.

[25] Robin Kellermann, Tobias Biehle, Liliann Fischer, “Drones for parcel and passenger transportation: A literature review”. Technical University Berlin, Department Work, Technology and Participation, Cluster Mobility Research, MAR 1-1, Marchstraße 23, 10587 Berlin, Germany.

[26] A. V. Clara and S. Redkar, “Dynamics of a vertical takeoff and landing (vtol) unmanned aerial vehicle (uav),” International Journal of Engineering Research & Innovation, vol. 3, no. 1, 2011.

[27] A. Vargas-Clara and S. Redkar, “Dynamics and control of a stop rotor unmanned aerial vehicle,” International Journal of Electrical and Computer Engineering (IJECE), vol. 2, no. 5, pp. 597–608, 2012.

[28] Zairil Zaludin, Ezanee Gires, “Automatic Flight Control Requirements for Transition Flight Phases When Converting Long Endurance Fixed Wing UAV to VTOL Aircraft”. IEEE International Conference on Automatic Control and Intelligent Systems (I2CACIS 2019), 29 June 2019, Selangor, Malaysia.

[29] B. L. Stevens and F. L. Lewis, Aircraft control and simulation. John Wiley & Sons, 2003.

[30] G. Cai, B. M. Chen, and T. H. Lee, Unmanned rotorcraft systems. Springer Science Business Media, 2011.

[31] *AirfoilTools*, 2015, [online] Available: http://airfoiltools.com/

[32] G. Ostojic, S. Stankovski, B. Tejic, D. Branislav, T. Nikola, “Design, control and application of quadcopter.” *International Journal of Industrial Engineering and Management*, vol. 6, pp. 43-48, 2015.

[33] A. A. J. K. Gunarathna 1 and S. R. Munasinghe, “Simultaneous Execution of Quad and Plane Flight Modes For Efficient Take-Off of Quad-Plane Unmanned Aerial Vehicles”, *Applied Science*, no. 1 (0), 2021.

[34] J. Anderson, Aircraft Performance & Design. McGraw-Hill Science Engineering, 1999.

[35] L. W. Traub, “Range and Endurance Estimates for Battery-Powered Aircraft.” *Journal Of Aircraft*, vol. 48, no. 2, pp. 703-707, Mar. 2011, doi: 10.2514/1.C031027.

[36] E. M. Greitzer and Z. S. Spakovszky, “Aircraft endurance,” in *Unified: Thermodynamics and Propulsion*, 2017.

[37] AT 3520-A _AT Series_Motors_Fixed_Wing_T-MOTOR Store-Official Store for T-motor drone motor, ESC, Propeller. [Online].
Available: https://store-en.tmotor.com/goods.php?id=794

[38] AT 75A 6S_ESC_Fixed Wing_T-MOTOR Store-Official Store for T-motor drone motor, ESC, Propeller. [Online].
Available: https://store-en.tmotor.com/goods.php?id=904

[39] “18x8 APC Propellers”. [Online]. Available: https://www.apcprop.com/product/18x8/

[40] MN5212 KV420_Navigator Type_Motors_Multirotor_T-MOTOR Store-Official Store for T-motor drone motor, ESC, Propeller. [Online]. Available: https://store-en.tmotor.com/goods.php?id=378

[41] ALPHA 60A 6S_ALPHA Series_ESC_Multirotor_T-MOTOR Store-Official Store for T-motor drone motor, ESC, Propeller. [Online]. Available: https://store-en.tmotor.com/goods.php?id=581

[42] P18x6.1 Prop-2PCS/PAIR_Polish_Carbon_Fiber_Propellers_Multirotor_T-MOTOR Store-Official Store for T-motor drone motor, ESC, Propeller. [Online]. Available: https://store-en.tmotor.com/goods.php?id=384

[43] “Tattu 15C 12000mAh 6S Lipo Battery Pack with EC5 Plug”. [Online]. Available: https://www.genstattu.com/tattu-12000mah-6s1p-15c-lipo-battery-pack-with-ec5-plug.html

[44] “Ardupilot”. *Open Source Drone Software. Versatile, Trusted, Open. ArduPilot.* [Online]. Available: https://ardupilot.org/

[45] A. Tridgell, H. Wurzburg and H. Willee (2016), “Quadplane Support”. [Online]. Available: https://github.com/ArduPilot/ardupilot_wiki/blob/master/plane/source/docs/quadplane-support.rst

[46] “McMaster-Carr,” *Mcmaster.com*, 2015. https://www.mcmaster.com/

[47] T V Baughn and P F Packman, “Finite element analysis of an ultra-light aircraft.” *Journal of Aircraft*. 23, 82-86, 1986.

# APPENDIX 1

A1.1. The code of the VTOL UAV has been forked from Ardupilots Github Repo and made necessary changes to suit the project. The code has been published in the team's Github Repo.

Link to the repo: https://github.com/Midhun-mannady/Final-Year-Project

A1.2. The public link to CAD files for the project's design is given below.

Link to the models: https://a360.co/36cNwOg

Password: *project*

# APPENDIX 2

The various MATLAB functions used to create the Simulink model are given below.

### A2.1. MOTOR MIXING ALGORITHM

```
function [Voltage, HVoltage] = fcn(Thrust, Throttle, Pitch,
Roll, Yaw)
Correct = 0;

if (Pitch/2+Roll/2+Yaw/2)>(100-Throttle)
    Correct=((Pitch/2+Roll/2+Yaw/2)-(100-Throttle));
end
if (Pitch/2+Roll/2+Yaw/2)>(Throttle-10)
    if Correct<((Pitch/2+Roll/2+Yaw/2)-(Throttle))
        Correct=((Pitch/2+Roll/2+Yaw/2)-(Throttle));
    end
end

if Correct~=0
    Pitch = Pitch-Correct/3*2;
    Roll = Roll-Correct/3*2;
    Yaw = Yaw-Correct/3*2;
end

Voltage = [(Throttle-Pitch/2-Roll/2-Yaw/2)*22.2/100
           (Throttle-Pitch/2+Roll/2+Yaw/2)*22.2/100
           (Throttle+Pitch/2+Roll/2-Yaw/2)*22.2/100
           (Throttle+Pitch/2-Roll/2+Yaw/2)*22.2/100];

HVoltage = Thrust*14.8/100;
```

### A2.2. VOLTAGE-FORCE CONVERSION

```
function [Torque, F, Current, HForce] = fcn(Voltage, HVoltage)
RPM = [0 0 0 0];
Torque = [0 0 0 0];
Current = [0 0 0 0];
F = [0 0 0 0];

for i=1:4
    RPM(i) = -1*10^(-13)*(Voltage(i)^3)-
(2.55*(Voltage(i)^2))+(340*Voltage(i))+(3*10^(-11));

    F(i) = 5*(10^(-9))*((RPM(i))^3)+(3*(10^(-
5))*((RPM(i))^2))+(0.124*RPM(i))-0.7793;
    Torque(i) = 8*(10^(-13))*((RPM(i))^3)+(9*(10^(-
9)))*((RPM(i))^2)+(2*(10^(-5))*RPM(i))-(7*10^(-5));

    Current(i) = 340*Torque(i);
end
```

```
HRPM = 7*10^(-12)*HVoltage^3-18.177*HVoltage^2+850*HVoltage-
4*10^(-8);

HForce = -4*10^(-11)*HRPM^3+6*10^(-5)*HRPM^2-
0.0338*HRPM+0.0054;
```

### A2.3. ROTATIONAL DYNAMICS

```
function RotAcceleration = fcn(Torque, F)
Moment=[0 0 0];
RotAcceleration=[0;0;0];
I=[0.1807 0.32154 0.4844];
Moment(1)=(F(3)+F(4))*0.301-(F(1)+F(2))*0.301;
Moment(2)=(F(3)+F(2))*0.5635-(F(1)+F(4))*0.5635;
Moment(3)=Torque(4)-Torque(1)+Torque(2)-Torque(3);
for i=1:3
    RotAcceleration(i)=Moment(i)/I(i);
end
```

### A2.4. LINEAR DYNAMICS

```
function Acceleration = fcn(F, HForce, Disturbance, Theta,
Velocity)
m = 6;
g = 9.81;
A = [0.184 0.17 0.63];
rho = 1.225;
Cd = 1;

Acceleration = [0 0 0];
Force = [0 0 0];
Fprop = [0 0 0];

Fprop(1) = sin(Theta(2))*cos(Theta(1))*(F(1)+F(2)+F(3)+F(4));

Fprop(2) = sin(Theta(1))*cos(Theta(2))*(F(1)+F(2)+F(3)+F(4));

Fprop(3) = cos(Theta(2))*cos(Theta(1))*(F(1)+F(2)+F(3)+F(4));

ThetaXY = -atan2(Fprop(1),Fprop(2));
XY2D = sqrt(Fprop(1)^2 + Fprop(2)^2);

if Fprop(3)>=0
    Fprop(1) = XY2D*sin(ThetaXY + Theta(3));
    Fprop(2) = XY2D*cos(ThetaXY + Theta(3));
else
    Fprop(1) = XY2D*sin(ThetaXY - Theta(3));
    Fprop(2) = XY2D*cos(ThetaXY - Theta(3));
end
```

```
if Velocity(1)<0
    Force(1) =
Fprop(1)+Disturbance(1)+0.5*rho*Velocity(1)^2*A(1)*Cd;

else
    Force(1) = Fprop(1)+Disturbance(1)-
0.5*rho*Velocity(1)^2*A(1)*Cd;
end

if Velocity(2)<0
    Force(2) =
HForce+Fprop(2)+Disturbance(2)+0.5*rho*Velocity(2)^2*A(2)*Cd;

else
    Force(2) = HForce+Fprop(2)+Disturbance(2)-
0.5*rho*Velocity(2)^2*A(2)*Cd;
end

if Velocity(3)<0
    Force(3) =
Fprop(3)+Disturbance(3)+0.5*rho*Velocity(3)^2*A(3)*Cd-m*g;

else
    Force(3) = Fprop(3)+Disturbance(3)-
0.5*rho*Velocity(3)^2*A(3)*Cd-m*g;
end

for i=1:3
    Acceleration(i) = Force(i)/m;
end
```

### A2.5. YAW ANGLE

```
function yaw = fcn(desty, destx)

yaw = atan2(destx,desty);
```

# APPENDIX 3

## SIMULINK MODEL OF THE FLIGHT CONTROL SYSTEM